

Hypogene speleogenesis related to porphyry magmatic intrusions and its influence on subsequent karst evolution in the Peruvian high Andes

Alexander Klimchouk^{a,*}, David Evans^b, Sasa Milanovic^c, Cristian Bittencourt^d, Mauro Sanchez^e, F. Carlos Aguirre^e

^a Institute of Geological Sciences, National Academy of Sciences of Ukraine, Kiev, Ukraine

^b FloSolutions, Lima, Peru

^c University of Belgrade, Serbia

^d HydroKarst, Curitiba, Brazil

^e Minera Antamina, Lima, Peru

ARTICLE INFO

Keywords:

Karst
Hypogene speleogenesis
Peruvian Andes
Antamina mine

ABSTRACT

Carbonate rocks of Cretaceous and Jurassic age are widespread in the Peruvian Andes where they host numerous magmatic intrusions and related ore deposits. Most of Peru's metal ore deposits are located at high elevations within a narrow, tectonized carbonate-rock belt extending over 2000 km in length. Many of the limestone formations are karstified and characterized by high recharge and percolation rates, well-developed subsurface drainage and complex flow patterns. Knowledge of karst in the Andes is generally limited, although karst is recognized to cause extreme hydrogeologic complexity and great challenges in development of mining facilities located in carbonate settings. Aspects of the origin of void/conduit systems (i.e. speleogenesis) and karst evolution are rarely addressed in environmental impact and risk assessment studies.

This study in the Antamina area in the east side of the Cordillera Occidental, home to the world largest known skarn copper-zinc deposit, demonstrates that the current karst system has formed as the result of polygenetic and multi-phase development. Structure-controlled hypogene cave systems are well-preserved and widespread in the area and present a foremost example of endogenous hypogene speleogenesis related to magmatic intrusions. Hypogene karst structures have strongly influenced subsequent epigene karstification, which commenced at the Pliocene-Pleistocene boundary. Changes in the base-level position due to the landscape evolution and Pleistocene glaciations were major additional factors that influenced epigene karst development. The findings of this study are potentially relevant to assessing karst origin and hydrogeology in many carbonate-hosted ore deposits in the Peruvian Andes and other regions. This study shows that the speleogenetic and evolutionary approach is indispensable in the development of sound conceptual models of groundwater flow in karst terrains and the assessment of karst-related hazards and risks.

1. Introduction

The development of mineral deposits hosted in carbonate rocks, especially in mountainous regions, is often challenging due to hydrogeological and engineering risks associated with karstification. Hydrogeological characterization of karstified terrains is difficult due to the extremely heterogeneous distribution of hydraulic parameters and the presence of highly conductive solution conduits, which transmit most of the flow (commonly 96–99 %; Worthington et al., 2000) but are difficult

to detect or predict, particularly in tectonized mountain settings. The standard investigation approaches based on drilling, hydraulic tests, and piezometer data, are commonly not successful due to the low probability of intercepting conduits by drill holes and the uncertainties regarding their patterns and the degree of connectivity of piezometers with the conduit system. The extreme heterogeneity of hydraulic properties and the poor understanding of the geometry and functioning of karst conduit systems limit the adequacy of numerical groundwater flow models and their predictive capacity.

* Corresponding author.

E-mail addresses: klimchouk@nas.gov.ua (A. Klimchouk), devans@flosolutions.com (D. Evans), sasa.milanovic@rgf.bg.ac.rs (S. Milanovic), cbittencourt@hydrokarst.com.br (C. Bittencourt), masanchez@antamina.com (M. Sanchez), caguirref@antamina.com (F. Carlos Aguirre).

<https://doi.org/10.1016/j.geomorph.2022.108488>

Received 6 August 2022; Received in revised form 15 September 2022; Accepted 9 October 2022

Available online 13 October 2022

0169-555X/© 2022 Elsevier B.V. All rights reserved.

The development of sound conceptual groundwater flow models for karst terrains, as well as the assessment of karst-related hazards and risks, critically depends on the understanding of the origin of conduit systems (i.e. speleogenesis) and related karst evolution (Klimchouk et al., 2000; Ford and Williams, 2007; Palmer, 2007; De Waele and Gutierrez, 2022; Evans and Waltham, 2022). Void/conduit systems of different origins have characteristically distinct spatial patterns and hydrogeologic functioning. The presence of karst features inherited from preceding phases of karstification may strongly influence groundwater flow and karst development in subsequent phases. However, aspects of speleogenesis and karst evolution are rarely addressed in applied karst investigations in mining areas.

In the Peruvian Andes, carbonate rocks of the Cretaceous and Jurassic age occur in two narrow, tectonized belts extending for over 2000 km along the main structures, covering about 13 % of the surface area (Fig. 1). These carbonate terrains, which are commonly karstified, are metallogenetically important as they host most major metal ore deposits occurring in the polymetallic skarn and carbonate-replacement belt of central Peru at elevations between 3500 and 5000 m. These deposits are related to igneous intrusions and associated interactions between hydrothermal fluids and host rocks (Love et al., 2004; Evans,

2015).

However, the published knowledge of karst in the Andes is generally limited and no systematic regional studies of karst and caves in the Peruvian Andes exist. The mining companies conducted a lot of research in karst terrains but their results are largely not available in the public domain. Karst is recognized to cause extreme hydrogeologic complexity and great challenges in the development of mining operations in karstic terrains, particularly with regard to mine waste management (Evans et al., 2005; Evans, 2015) and groundwater inflows to underground mines (Apaza-Idme et al., 2015). Recent speleological investigations were mostly focused at the Amazonas region with medium-altitude, wet tropical conditions (Guyot et al., 2014). Several significant caves are known in the high Peruvian Andes, including 2.8 km long Gruta de Huagapo in the Acobamba District and 638 m deep Sima Pumacocha in the Yauyos District (Pumacocha 2004 Expedition Report, 2019). A more thorough search in a part of the latter area (the Puyo Valley) resulted in the discovery of some 100 caves, mainly vertical shafts up to 190 m deep, at elevations between 4550 and 4800 m (McKenzie, 2012), indicating that intense karstification is common at high elevation carbonate belts of the Peruvian Andes.

Most of the applied studies of karst in mining areas *a-priori* implied that karstification was epigenic in origin, i.e. driven by the downward recharge from the exposed surface, developing within the contemporary geomorphic setting. When paleokarst is recognized, it is commonly assumed to form as epigenic karst during the ancient exposure epochs. Meanwhile, the geodynamic evolution of the Peruvian Andes, particularly the widespread Late Miocene (around 10 Ma) magmatism, numerous intrusions, and related hydrothermal events which affected Cretaceous carbonate sediments, could favor the formation of hypogene karst, i.e. the development of solution conduits by ascending fluids. It was recognized during the last decades that hypogene karst represents a special genetic type of karst, characterized by void-conduit systems distinct in patterns and functioning from more familiar epigenic karst (Klimchouk, 2007, 2015, 2017), and that it occurs globally much broader than previously believed (Klimchouk et al., 2017). The recognition and appreciation of the influence of hypogene karst on the contemporary hydrogeologic conditions and karst development are crucial to the development of adequate conceptual groundwater flow models and karst-related hazard assessments.

Although many cases of hypogene karstification are shown to be related to hydrothermal systems, studies of this type of karst directly associated with igneous intrusions are scarce. This paper demonstrates that structure-controlled hypogene conduit systems are well preserved and widespread at least in some parts the Antamina area in the eastern side of the Cordillera Occidental, which hosts the largest known copper-zinc skarn ore deposit. Caves in the area clearly exhibit the overprint of epigenic features over distinctly hypogene speleogens. Hypogene caves are not related to the present-day hydrogeologic, geomorphological, and climatic conditions but exert strong control on the contemporary groundwater flow, epigenic karstification, and geomorphogenesis. The Antamina study suggests that the inheritance of hypogene karst features, particularly those formed by intrusion-induced hydrothermal systems, can be the major factor influencing the contemporary karstification and hydrogeology associated with ore deposits in the Peruvian Andes and other regions.

2. Materials and methods

This paper is based on detailed field studies within a 13 km² area encompassing the Tucush Valley, located northeast of the Antamina's orebody, and the ridge that borders it in the northeast. This study was supplemented with cursory observations within a larger area extending 5–20 km from the site. Our site-specific studies employed specialized surface mapping, speleological/speleogenetic investigations, dye trace tests, and structural and geomorphological analysis of satellite (Google Earth) and drone imagery acquired during this study.

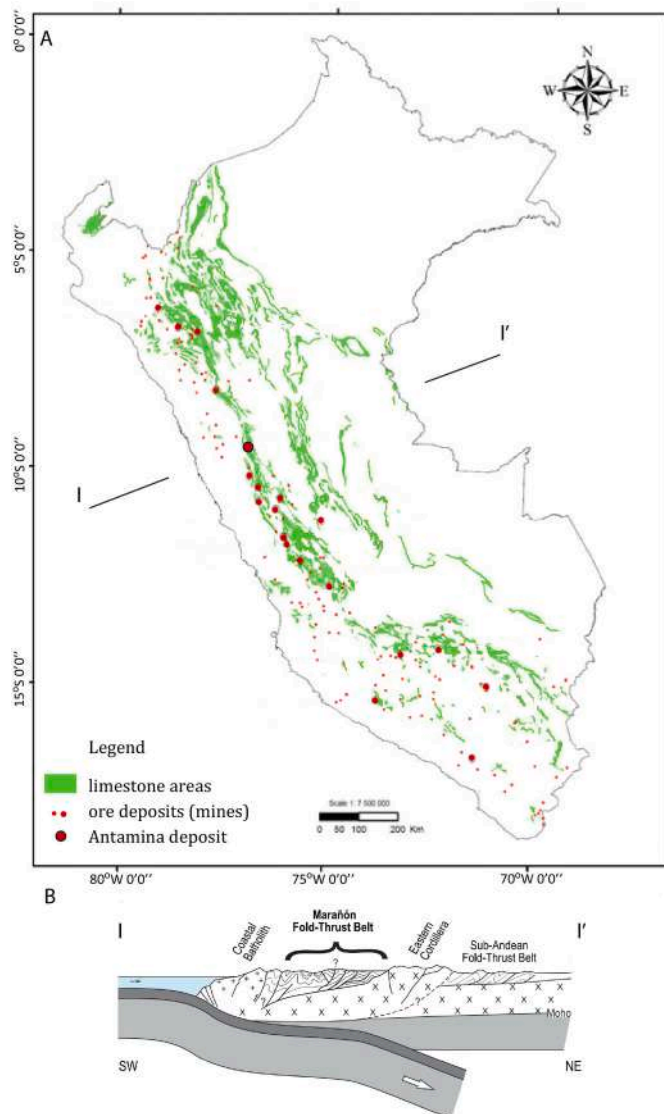


Fig. 1. Carbonate terrain and operating mines in the Peruvian Andes (A; modified from Evans, 2015) and (B) geodynamic situation of the Marañón Fold-Thrust Belt (Section 1–1'; adopted from Scherrenberg et al., 2014).

Specialized surface mapping, in addition to enhancing information about the distribution of karst features throughout the area, focused on revealing the main controls on the formation/location of karst features and attributes pointing to their origin, relative age and genetic relationships with regard to the contemporary denudation surface.

Speleological/speleogenetic investigations included: 1) exploration of caves identified during specialized surface mapping, and 2) detailed speleogenetic investigation/mapping of seventeen caves selected during the mapping phase. Speleogenetic investigation involved standard cave surveying using compass and clinometers (British Cave Research Association Grade 3C, <http://bcra.org.uk/surveying/>), observations on cave patterns and their relationships to structural and lithological features, identification and mapping of meso- and micro-morphological features indicative of certain conditions of formation (origin), based on criteria established in the specialized literature (Ford and Williams, 2007; Klimchouk, 2007, 2009a; Palmer, 2007; Audra et al., 2009a,b). According to the origin of features, dissolution surfaces of different origin were distinguished and mapped wherever possible. Cave investigations also included sampling and analysis of cave sediments and speleothems to aid speleogenetic interpretation. One sample of a calcite speleothem from a cave has been dated by $^{234}\text{U}/^{230}\text{Th}$ method in the Xi'an Jiaotong University Isotope Laboratory (Prof. Hai Cheng).

To enable a robust genetic interpretation of the acquired field speleological data and develop the evolution model for the Tucush karst system, the analysis of the geological, geodynamic, and geomorphological history of the region has been performed, based on the published accounts and available reports, as well as the analysis of site-specific geological and hydrogeological data from previous studies.

3. Regional geology and evolution

The Andes mountain belt is the result of the orogeny initiated in the Early Jurassic - a crustal deformation due to a flat subduction of the oceanic Nazca Plate under the continental South American Plate and crustal thickening of the overriding plate (Ramos, 2009). The plate collision resulted in the folding and faulting, uplift, volcanism, plutonism, hydrothermalism, and the formation of numerous mineral deposits that form the polymetallic belt of North Central Peru.

Antamina lies 30 km east of the crest of the Cordillera Blanca, the eastern one of the two main mountain chains comprising the Cordillera Occidental of North Central Peru, within the belt of the Albian - Upper Cretaceous carbonates stretching SE-NW in accordance with the regional structural framework (Fig. 2).

During the Late Jurassic through the Late Cretaceous, thick sediments were deposited in the eastern part of an extensional back-arc basin (the Western Peruvian Trough), located east of a magmatic arc (now the Coastal Zone and the Cordillera Negra. These sediments include slates and quartzites (Chicama Fm), deltaic sandstones, shales and coal with marine limestone (Goyllarisquisza Group), thick transgressive marine carbonates (Pariahuanca, Chulec, Pariatambo and Jumasha Fms), and marine shales with carbonates (Celendín Fm) (Lipten and Smith, 2005). After marine regression and uplift, continental red bed sediments were deposited in the Late Cretaceous and Paleocene.

Antamina is located within the generally north-northwest-trending Marañón Fold-Thrust Belt (MFTB) formed in the eastern part of the basin in the mid-Eocene through Oligocene due to extensive folding and reverse faulting (the Incaic phase of the Andean orogeny). It forms the core of the Cordillera Occidental and consists of highly deformed

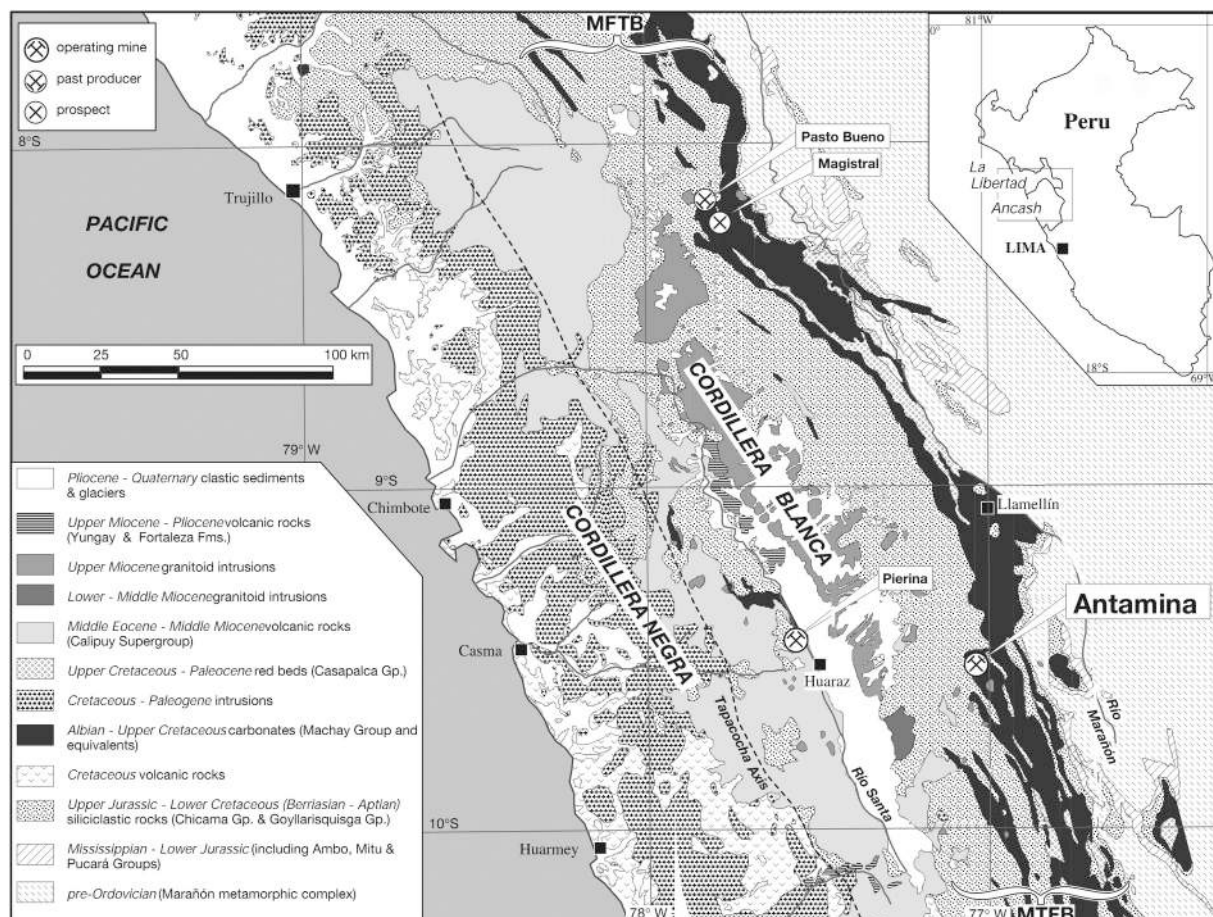


Fig. 2. The regional geologic setting and the location of the carbonate belt and the Antamina deposit (from Love et al., 2004). MFTB - Marañón Fold-Thrust Belt.

Cretaceous strata occasionally punctured by small Cenozoic plutons (Pfiffner and Gonzalez, 2013). Scherrenberg et al. (2014) show that the Chonta Fault, a long-lived, deep basement-rooted, NNE-trending pre-folding normal fault, was inverted during the Eocene and played an important role in dictating the spatial and temporal distribution of deformation in the fold-thrust belt. It separated the precursor back-arc basin geometry into two Cretaceous stratigraphic domains of different facies and thicknesses, and during the subsequent deformation, it controlled the transition between the two modes of thin-skinned behaviour (Pfiffner and Gonzalez, 2013; Scherrenberg et al., 2014). The Chonta Fault System is believed to play an important role in controlling subsequent Miocene intrusions and mineralization in the Cretaceous carbonate belt of the Ancash region (Villarreal et al., 2010).

Love et al. (2004) recognized a cross-strike (northeast-trending) structural discontinuity in the segmented MFTB called the Querococha arch, on which the middle Miocene Carhuish pluton, the Antamina stock, and a swarm of other intrusions lie. The arch is believed (Love et al., 2004) to reflect a transform segment of the originally jagged, rifted continental margin, which persisted as a transverse basement weakness that affected regional-scale sedimentation and structural patterns. In the Antamina area, these basement structures influenced lateral ramp formation and related fracture development in the overlying thrust sheets, localized later uplift and the rapid transit of small volumes of productive melt into a shallow crustal setting - conditions favorable for formation of a giant magmatic-hydrothermal ore deposit (Love et al., 2004). Scherrenberg et al. (2014) noted common occurrence through the MFTB of NE-SW-trending strike-slip faults that crosscut the regional NNW structural trend and may represent basement-involved transverse faults.

In the Middle to Late Miocene, the Cordillera Blanca batholith and numerous small igneous bodies were intruded in the eastern part of the Western Trough sequence in two to three events (Lipten and Smith, 2005; Pfiffner and Gonzalez, 2013). It is generally agreed that the Cenozoic intrusions in northern-central Peru originated primarily from partial melting in the lower crust thickened by crustal underplating (Petford et al., 1996), at a crustal thickness of >40–45 km, whereas igneous rocks have undergone limited midcrustal and shallow crustal assimilation (Bissig and Tosdal, 2009). Estimates of the Cordillera Blanca batholith emplacement depth vary from 7.5 km to 11.5 km based on pressure for the stability of mineral assemblages (Wise and Noble, 2003), although Cobbing et al. (1981) estimated 3 km paleo-depth of intrusion based on tectono-stratigraphic relationships. Wise and Noble (2003) prefer a variable paleo-depth of the main batholith intrusions between 3 and 7.5 km. Mrozek (2018) estimated the depth of the Antamina intrusions between 4.0 and 3.5 km, based on pressures derived from fluid inclusions.

The Antamina deposit formed at ca.9.5–11 Ma around a monzogranitic porphyry intrusion that pierced the Jumasha and Celendín carbonates (Love et al., 2004; Lipten and Smith, 2005; Mrozek et al., 2015, 2017; Mrozek, 2018). The last phase of the Cordillera Blanca batholiths took place between 8.2 and 6.3 Ma (Mukasa, 1984; McNulty et al., 1998), after which magmatism ceased (Love et al., 2004). Studies of the thermal evolution of exhumed and uplifted rocks in the region based on zircon fission track and (U-Th)/He dating of zircons (Garver et al., 2005) indicate moderate to rapid post-intrusive cooling in the Miocene and a high Miocene geothermal gradient (ca. 40°–50 °C/km). They note that this widespread cooling age represents a falling geotherm, not a period of significant exhumation.

The formation of the high mountain relief in the north-central Peruvian Andes is related to the Eocene compressive Inca Phase and particularly the post-Eocene extensional Quechua Phase folding and thrusting (Pfiffner and Gonzalez, 2013). Rapid and continuous exhumation of the Cordillera Blanca through both erosional and tectonic processes has occurred since 5–6 Ma (Perry and Garver, 2004; Garver et al., 2005). The latest phase of exhumation and canyon incision is ongoing and corresponds to the Cañon stage of erosion widely

recognized throughout this part of the Andes (Garver et al., 2005). The latter work estimates that 4.5–5 km of unroofing has occurred in high parts of the Cordillera Huayhuash and the Cordillera Blanca during this phase. Fission-track study by Garver and Rodbell (2002) indicates a denudation rate of 1.1 to 2 mm/yr for the last several million years. During the Pleistocene, repeated glaciations contributed significantly to the exhumation and shaping of the high mountain relief. Based on the depth of the Tucush Valley and a large glacial cirque north of it (Cheguia Lake) compared to the elevation of the surrounding peaks, glacial erosion in the area can be roughly estimated at up to 500 m.

4. Study area

4.1. Physiographic setting, glaciation, and climate

Antamina is located in north-central Peru, within the upper catchment of the Marañon River, a tributary of the Amazon River. The open-pit mine is situated at an altitude of 4300 m above sea level (masl) in a glacial valley. The area is characterized by rugged topography, with steep limestone ridges and mountain peaks ranging from 4300 to almost 5000 masl in altitude. The main ridges and valleys trend northwest, in accordance with the regional Andian trend structure, cut by shorter transversal, northeast-trending valleys, e.g. Antamina, Callapo, Ayash, and Cheguia Valleys (Fig. 3).

This study is focused on an area that lies northeast of the Antamina deposit, encompassing the 4.5 km long, northwest-trending U-shaped Tucush Valley and its ridge that borders the valley at the northeast. The elevations of the valley floor range from 4300 m to 4000 masl between the upper and lower reaches, and the surrounding ridges rise up to 4750 masl. The northeastern side is underlain by intensely karstified limestone extending through the ridge (Fig. 4) onto the opposite slope. In its lower reach, the Tucush Valley merges with the lower reaches of the much wider Huincush Valley, and both drain to the V-shaped transverse Ayash Valley, which runs northeast and deeply cuts the Tucush Ridge.

At least three phases of Pleistocene glaciations are recognized for the area, with the ice limit extending down to an elevation of about 3500 masl (Machare et al., 1990; Lipten and Smith, 2005), although the timing and the relative geomorphic roles of these phases are not well constrained. Moreover, the evidence for a cordilleran glaciation during the Pliocene was reported by Bonnot et al. (1988). There is an extensive record of glacier advances in the Cordillera Blanca that occurred at >50 ka (Hall et al., 2009). Evidence from the region, such as moraines dated at >400 ka, located down-valley of the Last Glacial Maximum (LGM) moraines and dated at >400 ka (Farber et al., 2005), indicate that the maximum ice volumes and extent of glaciers predate the LGM. There are systematic indications of an early LGM advance (34–27 ka; Clapperton, 1998), followed by a late glacial advance, and rapid deglaciation by ~20 ka (Zech et al., 2009; Mark et al., 2017). During the LGM, equilibrium-line-altitudes (ELAs) in the Cordillera Blanca during the LGM were depressed at 700–1000 m as compared to modern ELAs (Mark et al., 2017). The expansion of ice cover occurred between 18 and ~14 ka (the Oldest Dryas) (Mark et al., 2017), followed by a rapid deglaciation that took place between 14 and 10 ka (Machare et al., 1990; Seltzer, 1990).

In the Antamina Valley, two moraines are recognized (Lipten and Smith, 2005) although not dated. The first glacial event is believed to unroof the deposit and expose fresh sulfides, with the subsequent interglacial (recession?) period resulting in oxidation of the latter and the formation of ferricretes (Lipten and Smith, 2005). A prominent two-stage moraine sequence associated with the LGM is documented in different Peruvian ranges and appears well-correlated between them (Machare et al., 1990) so it is likely that the moraines in the Antamina Valley represent not separate glaciations but stages within the LGM. The moraine deposits in the Huincush Valley are referred to as a lateral moraine in the Antamina internal reports.

The climate of the tropical Andes is typical of low latitudes, where

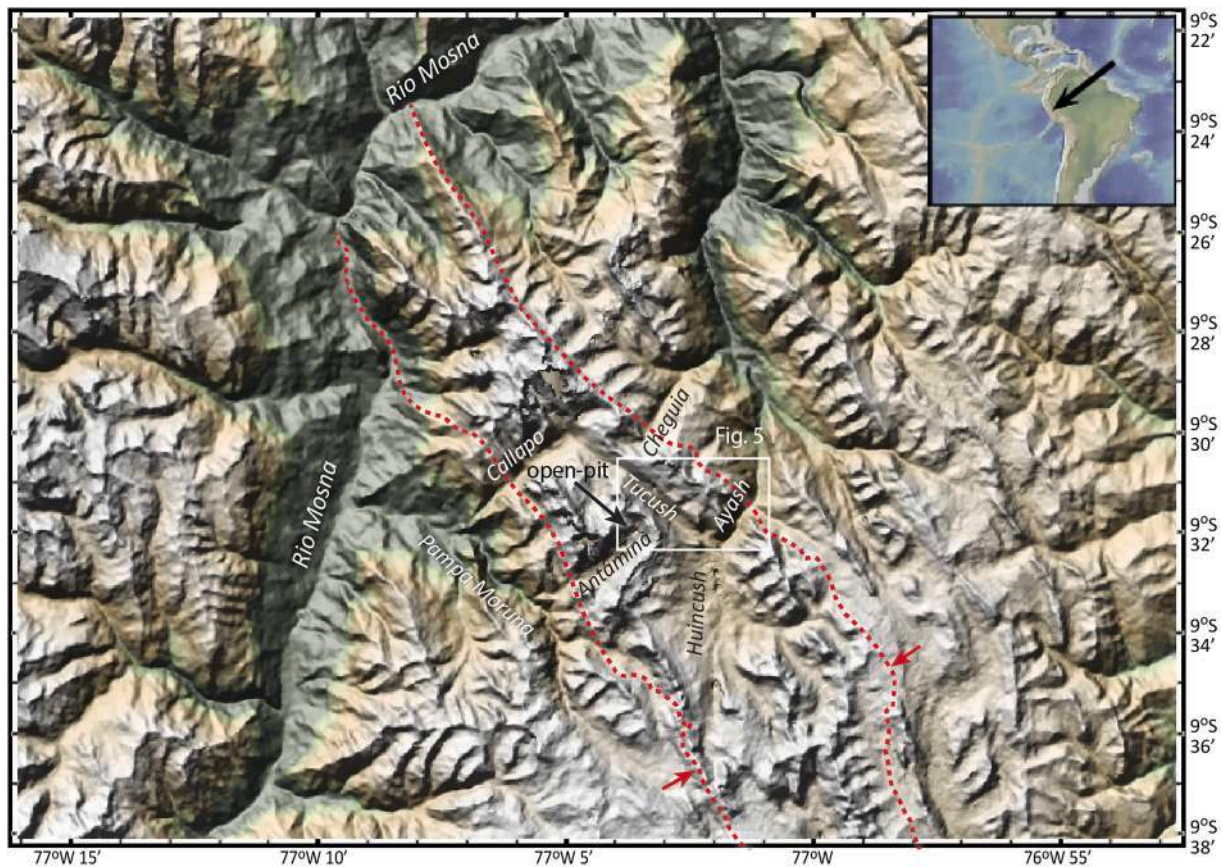


Fig. 3. Digital elevation model (from Global Multi-Resolution Topography data) showing the outer limits of the Jumasha limestone strip in the Antamina district (red dotted lines) and the location of the study area (the Tucush Valley and the ridge northeast of it – white rectangle) within the wider physiographic context. Prepared using GeoMapApp software. (For interpretation of the references to colour in this figure legend, the reader is referred to the web version of this article.)

the diurnal temperature range is greater than the annual range (Mark et al., 2017). Precipitation is derived mainly from moisture transported from Atlantic Ocean to the Andes via the easterlies (Garreaud et al., 2009). The average annual precipitation is approximately 1.1 m. There are two distinct seasons: 80 % of precipitation falls between October and March, April and September are transitional months, while the austral winter months of May to August are usually dry. Freezing conditions and snowfall can occur at any time of year but are relatively infrequent. Air temperature generally fluctuates between freezing and 15 °C, rarely dropping below −2 °C or exceeding 20 °C. Elevation plays an important role in the climate and precipitation distribution, producing several distinct microclimates within the area (Evans, 2015).

4.2. Geological setting

4.2.1. Stratigraphy

The Albian - Upper Cretaceous package of carbonate rocks encompassing the Antamina deposit and cropping out in the area is a part of the Machay Group, a succession deposited in the shallow-water portion of the Western Peruvian trough (Love et al., 2004; Fig. 2A). Predominantly siliciclastic sequence of the Upper Jurassic Chicama Group and the Lower Cretaceous (Berriasian to Aptian) Goyllarisquisga Group underlay the carbonate package. In the wider region, it is overlain by non-marine, coarse clastic red beds, not preserved in the immediate Antamina area. Cropping out in the area are Pariahuanca, Chulec, Pariatambo, Jumasha and Celendín formations of the Machay Group (Fig. 5).

Pariahuanca Formation (Ki-Ph) is composed of quartz sandstones with intercalations of black limestone and shale. The unit has an average thickness of 300 m.

Chulec Formation (Ki-Ch) is represented by laminar marl, intercalated with marlaceous limestones. The unit has an average thickness of 400 m and crops out along the northeast slope of the Tucush ridge.

Pariatambo Formation (Ki-Pa) is comprised by a package of predominantly dolomite with an average thickness of 180 m, in which the upper part has intercalations of black bituminous limestone.

Jumasha Formation (Ki-Ju1 to Ks-Ju4), is a limestone sequence with a total thickness of 1300–1500 m, in which four units have been differentiated: the Lower (Ju1), Middle (Ju2), Upper calcareous (Ju3) and the Upper marlaceous limestone (Ju4).

The Lower Jumasha (Ki-Ju1) is up to 650 m thick, represented by gray, thin to medium limestone beds intercalated with some yellowish dolomite beds and marly intervals. This unit outcrops along the upper northeastern slope of the Tucush ridge. The Middle Jumasha (Ks-Ju2) is about 500 m thick and is comprised of pure, light gray limestone with medium to coarse stratification (3–20 m), although some marly interbeds are also present. This unit comprises the upper-middle slopes of the Tucush Valley (Fig. 4). The top of the unit is marked by the so-called Sucesión Marcadora (Ks-Sm), a bituminous marly limestone unit 100 to 130 m thick. The Upper calcareous Jumasha (Ks-Ju3), cropping out along the middle slope of the Tucush Valley, is represented by predominantly dark gray thinly bedded limestone with an average thickness of about 100 m. The Upper marlaceous Jumasha (Ks-Ju4), varying in thickness from 150 to 200 m, is comprised of thinly stratified marly limestone and forms the top of the Jumasha Formation. Marly intervals that occur in all units of the Jumasha Formation are less resistant to erosion and often form well-defined strike-aligned troughs covered with vegetation (Fig. 4a, b).

Celendín Formation (Ks-Ce) exceeds 300 m in thickness and occurs in the lower slope and the base of the Tucush Valley, being largely covered

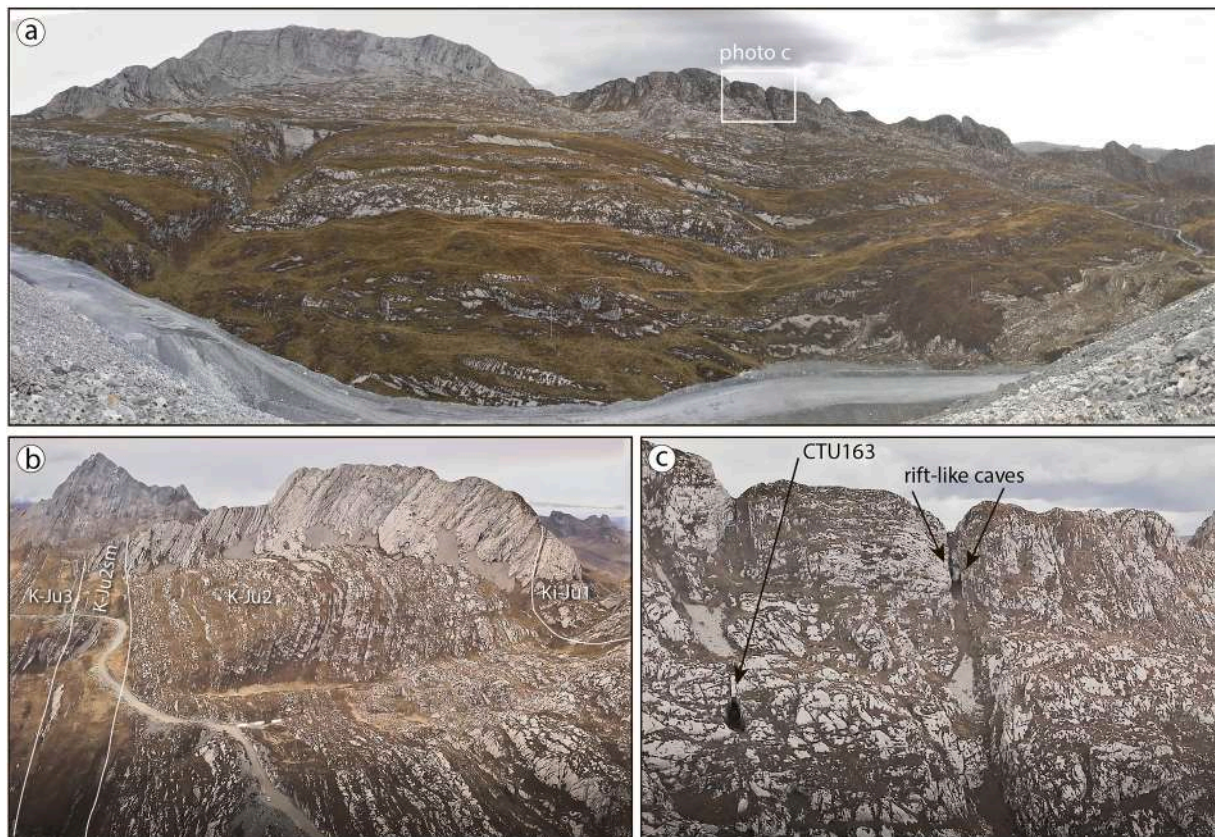


Fig. 4. A panoramic view to the Tucush Valley and ridge, looking to the northeast from the Antamina mine (a), an oblique drone view of the Tucush Ridge along the strike (b), and an oblique drone view of the upper parts of its slope. Note prominent transverse (NNE-NE-trending) linear landforms.

by Quaternary deposits and waste rock from the Antamina mine. It is comprised mainly of light gray, friable and laminated marl with some calcareous shale interbeds.

4.2.2. Structural setting

In the Antamina area, the Jumasha and Celendín Formations have been thrust-faulted, folded, and juxtaposed into a thick, complex thrust stack during the late Eocene Incaic orogeny (Love et al., 2004). In this stack, the NE-vergent thrust faults have a relatively shallow dip and are commonly crosscutting the bedding at a low angle. The regional high-angle Sacracocha Fault traces along the base of the Tucush Valley close to the Jumasha-Celendín contact and extends SE into the Huincush Valley.

Prominent northwest-striking, open, upright anticlines are exposed above the deposit on the northwest and southeast walls of the Antamina valley. The intervening synclines are tight. The Jumasha limestones in the Tucush area outcrop on the southwestern flank of the broad Ayash anticline and generally dip southwest at about 70°.

Minor dikes, sills, and skarn alteration zones extend beyond the main intrusion and orebody to the southwest down the Antamina Valley and to the northeast and east at the head of the valley, locally offsetting minor thrusts they cross (Love et al., 2004). Some of these dikes have minor Pb-Zn-Ag veins associated with them. Based on their distribution, Bodenlos and Ericksen (1955) describe a ca. 3 × 3 km area of dispersed hydrothermal activity centered on the Antamina skarn. We identified some dikes of the northeast strike crossing Jumasha limestones at the southwest slope of the Tucush Valley and in some caves.

Love et al. (2004) postulate the presence of underlying, northeast-striking basement faults beneath the Antamina area, which may have controlled some important local transverse features such as the Valley Lateral Ramp and associated vertical faults (the Valley Fault System), as well as numerous NE fractures. Northeast faults control important

present-day drainages in the Antamina area such as Río Puchca, Callapo, Antamina, Cheguia, and Ayash valleys (Fig. 3), discordant to the regional geologic strike. In the mine area, some segments of the contact between the main stock and the host limestones in Antamina form NE trending lineaments, suggesting that the valley-parallel faults played a role in controlling the intrusion and mineralization (Love et al., 2004). Our field survey shows that NNE- to NE-striking, large sub-vertical fractures with surface traces of 100–1000 m in length widely occur in the Jumasha limestones in the Tucush area (Fig. 5) and are of primary importance in controlling karstification. Love et al. (2004) interpret fractures of this set as tear fractures, formed by deformation associated with thrust translation along the underlying and similarly oriented transfer fault or lateral ramp. However, recent studies (SRK Technical Report, 2016) suggest that the cross-cutting faults may have been generated by multiple deformation (extensional reactivation) events late in the tectonic history, roughly coeval to the emplacement of the Antamina porphyry system.

4.2.3. Intrusions and mineralization

Antamina is a largest known skarn deposit in the world (Glencore, 2015) that occurs in and around a multiphase porphyry complex ranging in composition from quartz diorite to quartz monzonite. The main intrusion and skarn body is elongated NE-SW with dimensions in the plan view of ca. 2.5 km in length and ca. 1.5 km in width and includes several porphyry centers. It is over 2.2 km in the vertical dimension, from the highest elevation outcrop to the deepest drill core intersection, and remains open at depth (Mrozek et al., 2017). There is a nearby intrusion with narrow, weakly mineralized skarn 1.5 km northwest at Condorcocha and a smaller one 3 km north-northeast near Cheguia Lake. The Contonga and Taully stocks of quartz monzonite composition (300 m and 650 m in diameter respectively) are located 4 km north of Antamina intruding Jumasha limestones as subvertical cylinders of 300

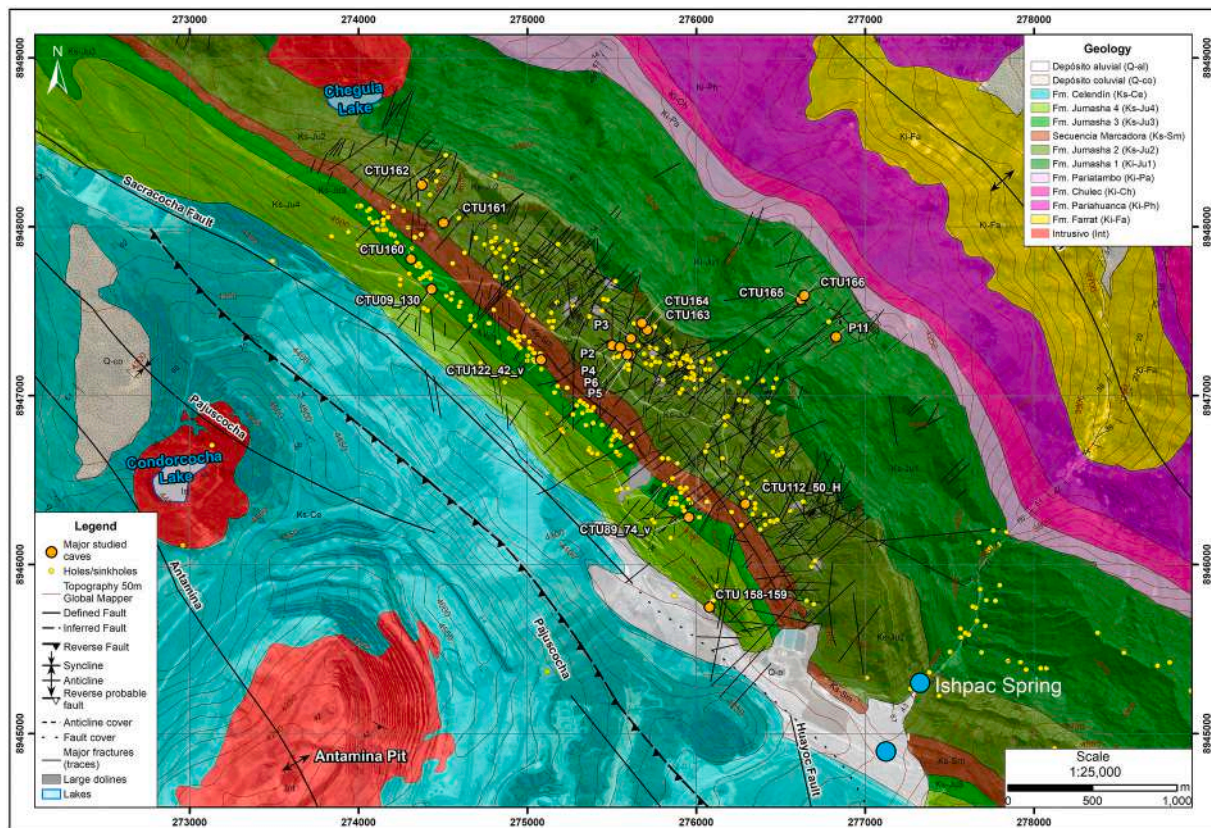


Fig. 5. Shaded geological map of the Tucush area (courtesy of Antamina Mine Company) showing traces of major fractures, distribution of large surface karst features, and locations of studied caves.

m and 650 m in diameter with a narrow ring of garnet skarn (Love et al., 2004). Yet another intrusive body is the Lucia pluton, a relatively large stock (4×2.5 km) of quartz monzonite and granodiorite with narrow garnet skarns which intruded Jumasha limestone about 7 km southeast of Antamina (Lipten and Smith, 2005).

The Antamina skarn consists of mainly garnet-bearing rocks and is symmetrically zoned around the intrusion (Redwood, 2004; Escalante et al., 2010). Subordinate hydrothermal breccia bodies (sheets and pipes) cut both the intrusion and skarn, mainly along structural weaknesses (Love et al., 2004).

Jumasha limestone around the skarn is altered to coarsely crystalline, gray to white calcitic marble that forms a tens to hundreds of meters wide aureole. According to Love et al. (2004), the outer limit of alteration in the Celendín Formation typically extends several hundreds of meters from the skarn boundary, although the halo represented by the swarm of Ag-bearing Pb-Zn vein deposits occur in both, the Celendín and Jumasha formations in a 9 km^2 area surrounding Antamina and up to a kilometer from the skarn front. The large-scale zonation of visible and cryptic (trace element content and oxygen isotope composition of the host rocks) alteration around Antamina is further demonstrated by detailed studies by Escalante (2008) and Escalante et al. (2010).

The heterogeneous distribution of marble, hornfels, and Ag-bearing Pb-Zn veins around Antamina is explained by fluid escape from the skarn through permeable fractures and certain sedimentary layers (Love et al., 2004; Escalante et al., 2010). The high volume of mineralized (endo- and exo-) skarn at Antamina suggests the production of high amounts of carbonic acid and CO_2 that got trapped in the skarn area by the coarse-grained marble envelope (Escalante et al., 2010) and the overlying Celendín Formation metamorphosed to hornfels (Love et al., 2004). Escalante et al. (2010) believe that the preferred pathways of the spent mineralizing fluids were quartz feldspar porphyry dikes, based on the presence of quartz and calcite + sulfide veins adjacent to them. They

note that low $\text{SiO}_2/\text{Al}_2\text{O}_3$ ratios of limestone around these features indicate no addition of silica in these rocks even in samples proximal to the dikes, suggesting a passive trace-element enrichment of the rocks close to the dikes mainly due to processes of carbonate dissolution. Trace-element halos to the quartz feldspar porphyry dikes extend farther than the thermal aureole of the Antamina skarn and reflect the interaction of progressively lower temperature fluids with carbonate rocks (Escalante et al., 2010).

Early dating of the Antamina intrusive complex using K-Ar, U-Pb (zircon) and $^{40}\text{Ar}/^{39}\text{Ar}$ (biotite) yielded ages between 10.4 ± 0.4 and 9.1 ± 0.4 Ma (McKee et al., 1979), at 9.75 ± 0.07 Ma (Love et al., 2004) and 10.94 ± 0.08 (Escalante, 2008). Recent studies by Mrozek et al. (2015, 2017) and Mrozek (2018) yielded new U-Pb (zircon) ages between 10.95 ± 0.20 Ma and 10.24 ± 0.23 Ma and Re-Os (molybdenite) ages ranging from 10.58 ± 0.07 Ma to 9.68 ± 0.05 Ma. Zircon ages record early-stage magma crystallization at temperatures around 900°C or higher, whereas Re-Os ages correspond to molybdenite deposition at hydrothermal conditions ($<450^\circ\text{C}$) (Mrozek, 2018). The latter study constrains the duration of magmatic-hydrothermal activity in Antamina to 1.52 Ma. Based on cross-cutting relationships of main intrusive centers and various sub-bodies (dikes, veins, etc.), three major intrusive phases and at least eleven sub-phases are distinguished (Mrozek et al., 2015, 2017; Mrozek, 2018).

4.3. Hydrogeologic setting

The karst hydrogeological system of the Tucush valley and ridge has been studied thoroughly since 2002 by the Antamina Mining Company and its contractors, most notably by Itasca (Itasca Technical Report, 2003), Schlumberger Water Services (2011–2013; SWS Technical Report, 2013) and FloSolutions (2019, this study). The structure and functioning of the system are primarily determined by lithostratigraphy,

stratigraphic and tectonic discontinuities, landscape, and karstification. The geological units of the Jumasha Fm. are characterized by a pronounced layering with beds of limestone alternating with marly limestones and marls. Bedding planes, dipping to SW at 70°–80°, are locally hydraulically activated by strike-parallel (N130°–N140°) fractures. Transverse tectonic discontinuities include high-angle (70°–90°), N- to NE-oriented fractures, of which fractures trending at N30°–N50° are particularly prominent and widespread. Karstification follows all these discontinuities to varying extent.

The Jumasha carbonates in the Tucush area are bounded on both sides by the lower permeable, impure carbonate formations - Pariatambo to the northeast and Celendín to the southwest (Fig. 5). The upper part of the Ayash Valley cuts across the Jumasha Formation to elevations of 3900–3850 m and provides the main local drainage base level for groundwater flow and karstification. Its draining influence extends to the northwest (strike-parallel) almost to the Cheguia Lake area, as indicated by groundwater tracing studies. Further to the northwest, the groundwater flow is drained by the cross-cutting Callapo and much deeper Rio Mosna-Puchca valleys. Discharge to the Ayash Valley from the Tucush area focuses in Ishpac Spring located on the west side of the upper Ayash Valley, which discharges from a karst conduit at 3900 m situated about 8 m above the Ayash River bed. During the wet season, there are discharges in the river bed along the Ayash canyon as indicated by substantial flow gains along some stretches. The average flow in the upper stretch is 2470 L/s in the wet season and 433 L/s in the dry season, indicating strong seasonality. The Ishpac Spring and other smaller discharges in the Ayash Valley respond to precipitation events within a matter of hours, but dry up completely after prolonged dry periods indicating that its hydraulic functioning is governed by an overflow process.

Groundwater recharge on the south side, base and lower slope of the Tucush Valley, largely underlain by marls and marly limestones of the Celendín Formation, is minor in comparison to recharge rates to the Jumasha. Most of the recharge in the Jumasha occurs throughout the middle-upper slopes of the valley and the northeast flank of the Tucush ridge (Ks-Ju2 and Ks-Ju1 units), within the karstified outcrops where rainfall quickly infiltrates into the epikarst zone. The epikarstic zone, though underdeveloped and irregularly distributed, is efficiently drained to the phreatic zone by well-developed karst shafts of various origins. The thickness of the vadose zone varies between 30 and 40 m in the valley bottom/lower slope to 190–465 m across the Tucush ridge, depending on the topography variations.

Analysis of the piezometric data and results of tracing tests reveals substantial compartmentalization of the Jumasha aquifer in the transverse (SW-NE) cross-section, determined by the presence of the lower-permeability marker horizon Sucesión Marcadora (Ks-Sm) comprised of marl and marly limestone. The Middle Jumasha (Ks-Ju2) and the Lower Jumasha (Ks-Ju1) units that comprise the Tucush ridge and host the main aquifer are most intensely karstified and deeply drained by the Ayash canyon, whereas the Upper Jumasha units (Ks-Ju3 and Ks-Ju4) in the lower Tucush slope are separated to some extent from the main aquifer by the Sucesión Marcadora. However, the barrier function of the Sucesión Marcadora appears to be compromised along transverse tectonic discontinuities and karst conduits, as suggested by some tracing results.

Piezometers installed in boreholes throughout the area show very different behaviour, varying from a fast and peaked (“flashy”) reaction to rainfalls, slow and smoothed (or flat-topped) to no reaction at all. Some piezometers show changes in behaviour between years. These variations may reflect: 1) different position of piezometers in the complex (double-triple) porosity systems (matrix + small fracture reservoir vs conduit system), 2) hydraulic compartmentalization due to faults, geologic contacts, and/or marly units, and 3) dynamic changes in degree of sediment infilling within karst conduits.

Hydrogeological studies to date show that groundwater movement in the phreatic zone in the Jumasha Formation is principally parallel to the

formation strike toward the Ayash canyon. Dye tracer tests reveal the existence of strike-parallel preferential flow systems stretching along both sides of the Sucesión Marcadora. Tracer tests conducted in the wet season, in which tracers were introduced directly into the conduit system, show very high flow velocities between 3700 and 5064 m/day - roughly two times the median velocity of conduit flow in karst (1940 m/day) derived from 3000+ tracing tests conducted in various regions of the world (Worthington and Ford, 2009).

In summary, the analysis of the available hydrogeological data suggests that the main aquifer in the Tucush area (Ks-Ju2 – Ks-Ju1) discharges to the Ishpac Spring and the Ayash River and is characterized by multiple porosity/permeability (mixed diffuse/conduit flow), low regulating capacity, low epikarst storage, and substantial compartmentalization along phreatic flow paths. Recharge in the Ks-Ju3/Ks-Ju4 units discharges mainly to the TSF dam and seepage collection system, although some losses to the main aquifer occur across the Sucesión Marcadora.

5. Surface karst features

Surface karst features of varying origins commonly occur throughout the Jumasha Formation but with uneven distribution. Some surface karst features are related to epikarst morphogenesis (Klimchouk, 2004) whereas others represent exhumation and adaptation of underground voids and conduits as the surface lowers by denudation.

The development of epikarst (the uppermost weathered/karstified zone with substantially enhanced and more homogeneously distributed porosity and permeability, as compared to the bulk rock mass below; Klimchouk, 2004) is strongly influenced by lithological variations (alternation of massive beds and thin-bedded marly packages), high-angle dip of beds, and the presence of pre-formed shafts that provide vertical drains down through the vadose zone. Epikarst is more uniformly developed within the outcrops of thick limestone packages of the K-Ju2 unit in the upper slopes of the valley where bedding control of the rock dismemberment is apparent (Figs. 4a, b; 6a). One- to five meters thick marl interbeds that regularly occur in this unit are preferentially eroded and form strike-aligned, soil-covered corridors bounded by protruding limestone beds (Figs. 4b; 6b). Local surface runoff and subcutaneous flow within such corridors dissolve lateral notches in the bounding beds. Vertical drainage through the vadose zone beneath epikarst occurs predominantly along transversal (NE-trending) fractures and pre-formed shafts associated with them.

In the middle-lower slopes, wide (50–100 m) strips of several meters-thick regolith (including organic-rich topsoil) formed over marly sub-units of the K-Ju4 and K-Ju3 units and the Sucesión Marcador member of the K-Ju2 unit, where no epikarst is directly exposed (Fig. 4a).

Epikarst in the Tucush area appears to be young and immature, which is suggested by its small thickness (typically 2–4 m, from observations in road cuts and karst shafts), low to moderate degree of rock blocks dismembering, and the scarcity of typical solution dolines and young vadose shafts that develop as an integral part of epikarst morphogenesis and are indicative of a mature stage of the epikarst formation (Klimchouk, 2004, 2009b; Bauer et al., 2005).

Distribution of major karst features in the Tucush area is shown in Fig. 5. The map shows them underrepresented within the Ki-Ju1 unit (the NE slope of the Tucush ridge) as this area has not been mapped in detail due to limited access. The category of holes/sinkholes (yellow dots) conventionally includes open holes (shaft/cave entrances and gaping crevices) and doline-like features, most of which show clear signs of being formed through exhumation of the void/conduit system (shafts, passages, chambers, enlarged fractures, etc.) (Fig. 6d–k). These exhumed karst features are not functionally adjusted with the current landscape, unlike true solution dolines that form by gradual surface lowering due to focused drainage and dissolution along draining fractures. True solution dolines are scarce and small in the Tucush area. Many exhumed caves are plugged by sediments at shallow depth.



Fig. 6. Typical surface karst features in the Tucush area: a–c – karstified outcrops (epikarst); d–k – exhumed caves and associated sinkholes. Most of features are distinctly controlled by NE-trending fractures (highlighted by red dashed lines in some photos). (For interpretation of the references to colour in this figure legend, the reader is referred to the web version of this article.)

Features that extend several meters in depth are classified as caves (shafts).

Exhumed caves occur in all units of the Jumasha Formation including the marly Sucesión Marcadora. Most of them are related to vertical shafts of fracture-controlled (rift-like) or circular/oval shapes in plan, decapitated or/and unwalled by the surface lowering (Fig. 7a–c). The vast majority of them are structurally controlled by transverse (NE-trending) fractures. Exhumed caves occur in any position in the modern landscape including crests of ridges (Fig. 7a), and have no or only minor associated depression or connection with larger surface water catchments. These relationships of the surface geomorphology and caves strongly suggest that the modern landscape is relatively young, that surface karstification is immature, and that caves were chiefly formed prior to the contemporary phase of the landscape and epikarst development.

Besides numerous dolines of metric to decametric size, chiefly formed through exhumation of caves, there are several large depressions in the Tucush area, shown in Fig. 7g–h. They are up to 150–200 m in width and up to 400 m in length and are elongated in the NE direction, which indicates the control by the transverse discontinuities and respective preferential underground karstification controlled by the latter. These features are commonly infilled by low-permeability soils.

Other prominent surface karst features in the Tucush area are large corridors controlled by large NE-trending fractures (Fig. 7d–f). They can be up to 10 m wide, assume the form of slot canyons in some sectors and

can be traced for several hundreds of meters in length.

6. Karst void/conduit system

Solution cavities, varying in vertical size between several centimeters to, in few cases, a couple of meters, have been regularly detected by drilling in the Tucush Valley. In one case, an open cavity > 3 m in height was intercepted at depth of 295 m. Substantial losses of drilling fluids has occurred during the drilling of several geotechnical and hydrogeological test holes within the Jumasha limestones.

In 2013, the hydrogeological team of Antamina started a speleological program to explore accessible caves and other karst features, within which over 100 objects were documented (see Fig. 5) and morphological signs of possible hypogene origin were noticed in some caves (Antamina Technical Report, 2015). Although most of these features are shallow pits blocked at the bottom, several are more complex, deeper caves. In 2018, this speleogenetic study was performed, during which seventeen significant caves were investigated in detail. Plans and profiles of some representative caves are shown in Figs. 8 and 9, their key morphological features are shown in Figs. 10–12, and brief descriptions are given in the Appendix. Sections of the cave contours with the abundance of rising flow features are indicated in profiles and plans of the studied caves as “hypogene dissolution surfaces” (Figs. 8 and 9).

Most caves with rising flow features are cascading vertical shafts that cross stratigraphy, although some cave elements are formed along

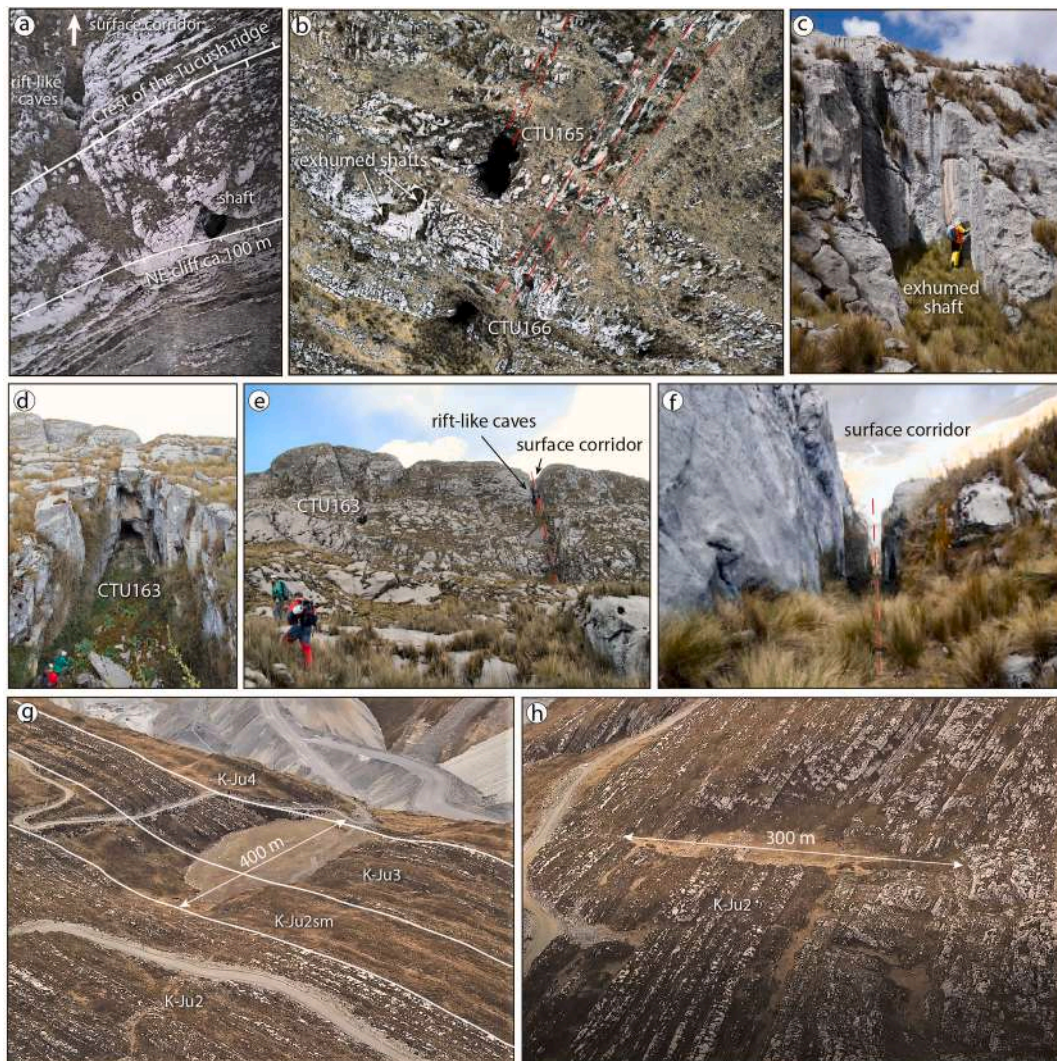


Fig. 7. Surface karst features formed due to exhumation of underground voids and conduits (a–f), and large dolines (g–h). Photos a, b, g, and h are oblique drone views. Photos a–c show beheaded/unwalled shafts (note that a shaft and rift-like caves in photo a are located proximal to the crest of the ridge). Photos d–f show slot-like surface corridors and photos g and h show large-scale dolines. Red dashed lines in b indicate large NE-trending fractures, white lines in g indicate contacts between the Jumasha Fm units. (For interpretation of the references to colour in this figure legend, the reader is referred to the web version of this article.)

bedding planes. Individual shafts are formed along large vertical fractures, which are offset vertically and laterally relative to each other but connected by inclined conduits formed along stratabound fractures and bedding joints. Rising-flow features are particularly distinct and form remarkable assemblages at upper sections of individual shafts (Fig. 10c–f). They are also common in tube-like inclined conduits that connect shafts at different levels (Fig. 11h–j). Several caves consist solely of such inclined conduits (e.g. CTU112 and CTU163; Fig. 9), with the upper shafts being destroyed by denudation and the lower shafts blocked by speleothems or breakdown rubble. Three caves contain large chambers with abundant rising-flow features; one is breached by a vadose shaft (CTU166; Fig. 8a), another one is breached by a cascade shaft with mixed vadose and rising-flow morphologies (CTU89; Fig. 8d), and the third one is truncated at the top by the denudational surface (CTU164; Fig. A1c).

Caves with rising-flow features scatter through the entire area and occur in all units of the Jumasha Formation. The distribution of such sections in the vertical profile along the Tucush ridge (Fig. 13) does not demonstrate any preferential altitude interval of their occurrence. This figure shows that rising flow features occur within the vertical range of at least 300 m.

Epigene (vadose) shafts are also frequent. In the studied caves, they

are formed through the superposition of the vadose flow over relict rising-flow shafts, variably modifying the latter. Vadose overprint is commonly evident in the middle and lower parts of individual shafts (Fig. 13d–e), although some open shafts have vadose morphology over the entire depth. In CTU09 (Fig. 8b), a large 95 m deep shaft has distinct vadose morphology with strictly vertical surfaces and vertical grooves. However, numerous remnants of pre-existed cavities with rising-flow morphology, cut at various levels by the vertical vadose surface, are clearly recognizable along the entire depth of the shaft (Fig. 12a, b). Some of such pre-existed cavities represent side feeders of a former rising-flow shaft now largely reworked by the vadose dissolution (Fig. 12b). In CTU166 (Fig. 8a), a large vadose shaft breaches into a chamber at the bottom with abundant rising-flow features (Fig. 13c).

In the studied caves, various calcite speleothems associated with vadose (subaerial) environments have been observed but no speleothems of phreatic origin were found. Flowstones of different morphological varieties are the most common type of speleothems. They occur as a simple sheeting less than a centimeter in thickness but often form crusts with a thickness of several decimeters and locally large and morphologically complex assemblages including cascades, canopies, etc. Flowstones and various dripstones (stalactites and stalagmites) are actively forming in some locations but in most cases, they are inactive

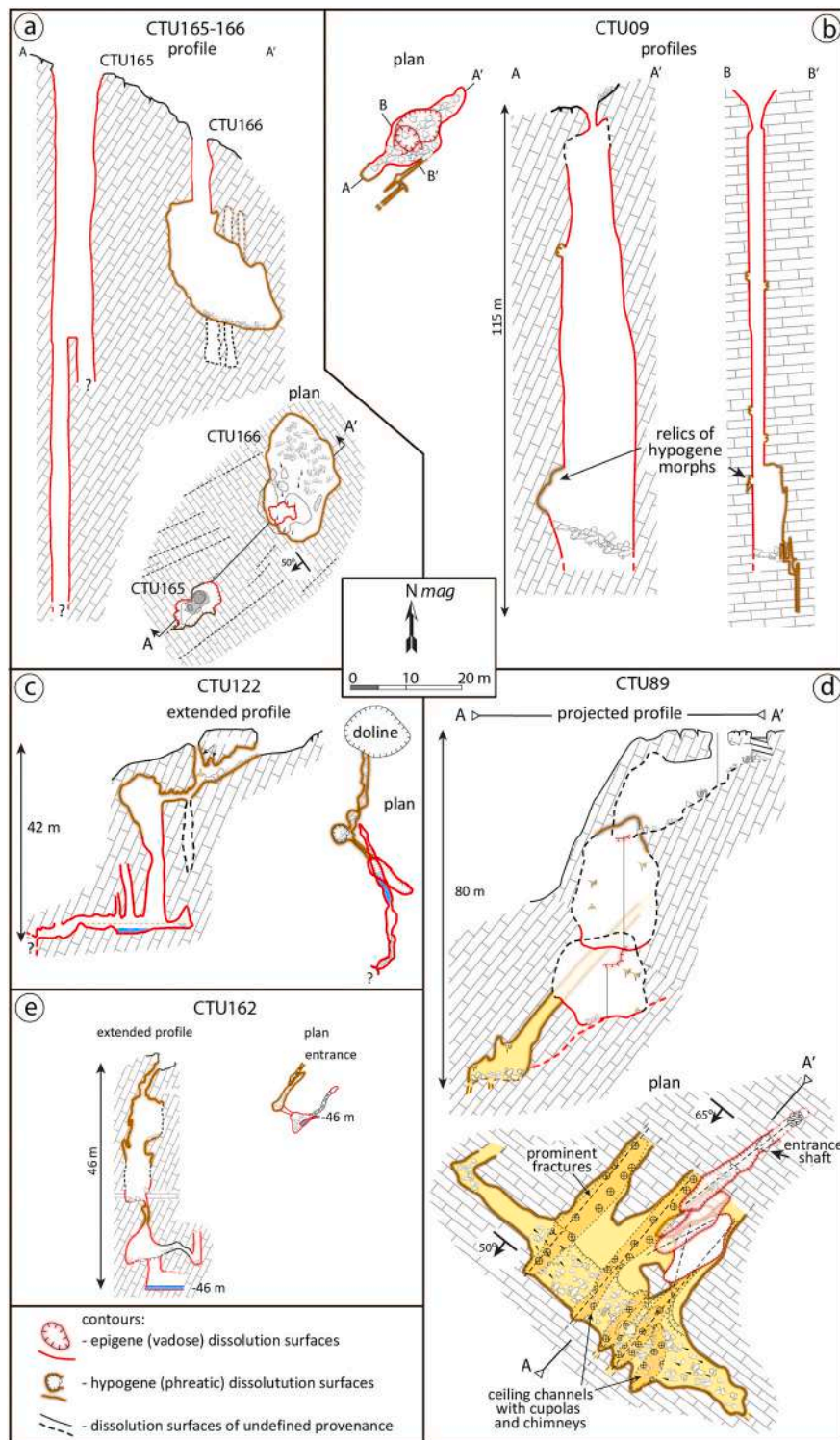


Fig. 8. Profiles and plans of vertical caves in the Tucush area showing sections with prevalent epigene (vadose) and hypogene dissolution.

and look old. Calcite from a massive flowstone canopy at the bottom of a rising-flow shaft truncated by the surface (CTU122) has been sampled and dated by the $^{234}\text{U}/^{230}\text{Th}$ method to be older than 700 ka (details of the analysis are given in Appendix 2). Flowstones of seemingly the same generation are found in internal shafts of some other caves (e.g. CTU89).

Also common are coatings of white to yellowish, sometimes powdery, calcite covering cave walls or other speleothems. In places, this calcite mass appears as dried moonmilk but in other cases, it has small crystals or coralloids on the surface. The same calcite constitutes (or

coats only?) massive deflected stalactites found some 15–20 m from the entrance in CTU112 cave. Larger ones have up to 1.4 m in diameter at the base and protrude for up to 2 m. These stalactites are inclined toward the cave interior which likely indicates a strong air draft in the past.

In the ceiling of the main chamber at the bottom of CTU89, up to 5 cm thick “crust” of ferruginous material has been found that once filled a steeply dipping bedding plane, now exposed. Strictly speaking, this is not a cave formation because the emplacement of this mineralization clearly pre-dates the main phase of speleogenesis as evidenced by rising

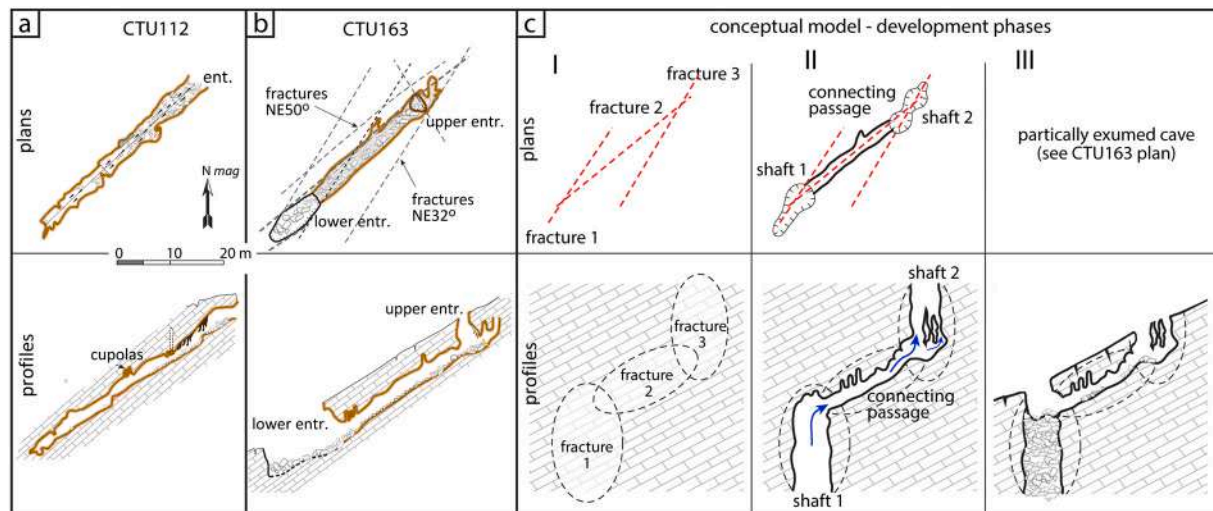


Fig. 9. Plans and profiles of CTU112 and CTU163 caves (a and b) represented by inclined passages, and a conceptual model of their formation (c). The initial setting (I) shows two vertically extended fractures, occurring with the vertical and lateral offset (fractures 1 and 3), connected with laterally extended stratabound fractures or bedding-plane joints. Ascending flow formed shafts along fractures 1 and 3 and an inclined passage along the connecting fracture 2 (II). Denudational lowering of the surface and collapses of larger cavities led to the present-day configuration of the partly opened karst system (III).

flow morphs of the cave digging under the ferruginous “crust”. Spectrometry analysis by the Terraspec instrument has shown that the mineral assemblage of this material is dominated by beidellite, siderite, and opaline silica, with Fe-oxides present such as goethite and hematite.

No fluvial sediments related to stream flows were found in the investigated caves. In several shafts that support vadose flow (e.g. CTU122 and CTU162), considerable accumulations of clay (residual?) in the vertical walls were observed. The clay forms a coating up to 0.5 m in thickness and is weakly cemented by calcite. In the bottom areas of some shafts, the clay accumulates in the floor and coats the walls within periodically water-filled pools, with clear marks indicating the water level.

A large mass of finely laminated, dry gray clay with a minimal thickness of 0.5 m was found along the wall of the inclined passage of CTU112 cave. This sediment seems to be rather old and was deposited in slow-moving or stagnant water. Pieces of the same clay, but almost lithified are found attached to the opposite wall. Spectrometry analysis by the Terraspec instrument has revealed the mineral assemblage consisting of beidellite, quartz, opal, and siderite. A similar but wider mineral assemblage was identified in a yellow clay-powdery material that filled a dissolution pocket in the wall at the bottom of the entrance shaft in CTU122 (beidellite, siderite, illite, allophane, opaline silica, and Fe-oxides such as goethite and hematite). The mineral composition of these clays relates them to the above-described ferruginous material that filled an enlarged bedding plane in CTU89.

Gravitational (collapse) deposits, represented by rock boulders and slabs of various sizes, are common in the near-entrance parts of inclined caves, in surface forms associated with unroofing of caves, and in chambers breached by shafts.

7. Discussion

7.1. Speleogenesis

Vertical shafts of different origins overwhelmingly dominate among documented caves in the Tucush area. They occur in all units of the Jumasha Formation and demonstrate strong structural control by transverse fractures (i.e. fractures having a N to NE orientation), although some elements are also controlled by bedding joints and strike-parallel fractures (N130° – N140°). Transverse fractures play the most important role in the karst development and groundwater flow from the

epikarst zone through the thick vadose zone to the water table.

All studied caves exhibit compelling and abundant morphological indications of rising flow, including various features (speleogens) organized in easily recognizable, spatially and functionally related assemblages. Such assemblages are generically termed “*morphological suites of rising flow*” (MSRF) and are shown to be strong evidence of hypogene karstification (Klimchouk, 2009a, 2019). They include feeders (orifices of rising flow conduits connecting into a given cave space), rising channels in hanging walls, smooth and sharp-edged solution pockets in the walls, rising ceiling channels with series of cupolas, nested cupolas and rising chimneys, bell-holes, and ceiling rock pendants (Figs. 9–11). The occurrence of these features in spatially related assemblages unambiguously indicates the formation by rising flow with substantial natural convection effects.

Such morphological features can be created by flow rising from deep tiers of phreatic conduits in places where discharge occurs in epigene karst systems. However, caves with such forms would be localized along paleo-discharge zones and within a restricted vertical range. Also, some rising flow speleogens can be created in epigene karst systems due to the sediment filling of conduits in the epiphreatic zone, which diverts flow to the ceiling area and causes upward-pointed dissolution during high flow and water table rise events (paragenesis). Since rising flow features in the studied caves are observed in shafts, occur within a > 300 m elevation range (Fig. 13), and scatter through the entire Tucush area, it can be safely ruled out that they are related to local paleo-discharge zones of the phreatic flow rise or to paragenesis in epigene karst systems. This is further corroborated by the wide occurrence of speleogens associated with natural convection, requiring sluggish dynamics of forced flow in hydraulically confined conditions, which is uncommon for dynamic epigene phreatic systems. In the study area, there were no region-wide and high-amplitude base-level rises that could cause the so-called *per ascensum* speleogenesis and the development of the vauclusean type shafts (e.g. Mediterranean Basin during and after the Pliocene transgression that followed the Messinian Salinity Crisis and the respective low base-level period (Audra et al., 2004)). Even in such cases, ascending shafts are localized along the discharge zones rather than scattered throughout the mountain area.

Yet another potential mechanism to generate rising flow features, similar to those observed in the Tucush caves, is condensation-corrosion which involves air convection. However, this mechanism may operate just above the thermal water table and/or where H₂S is available to

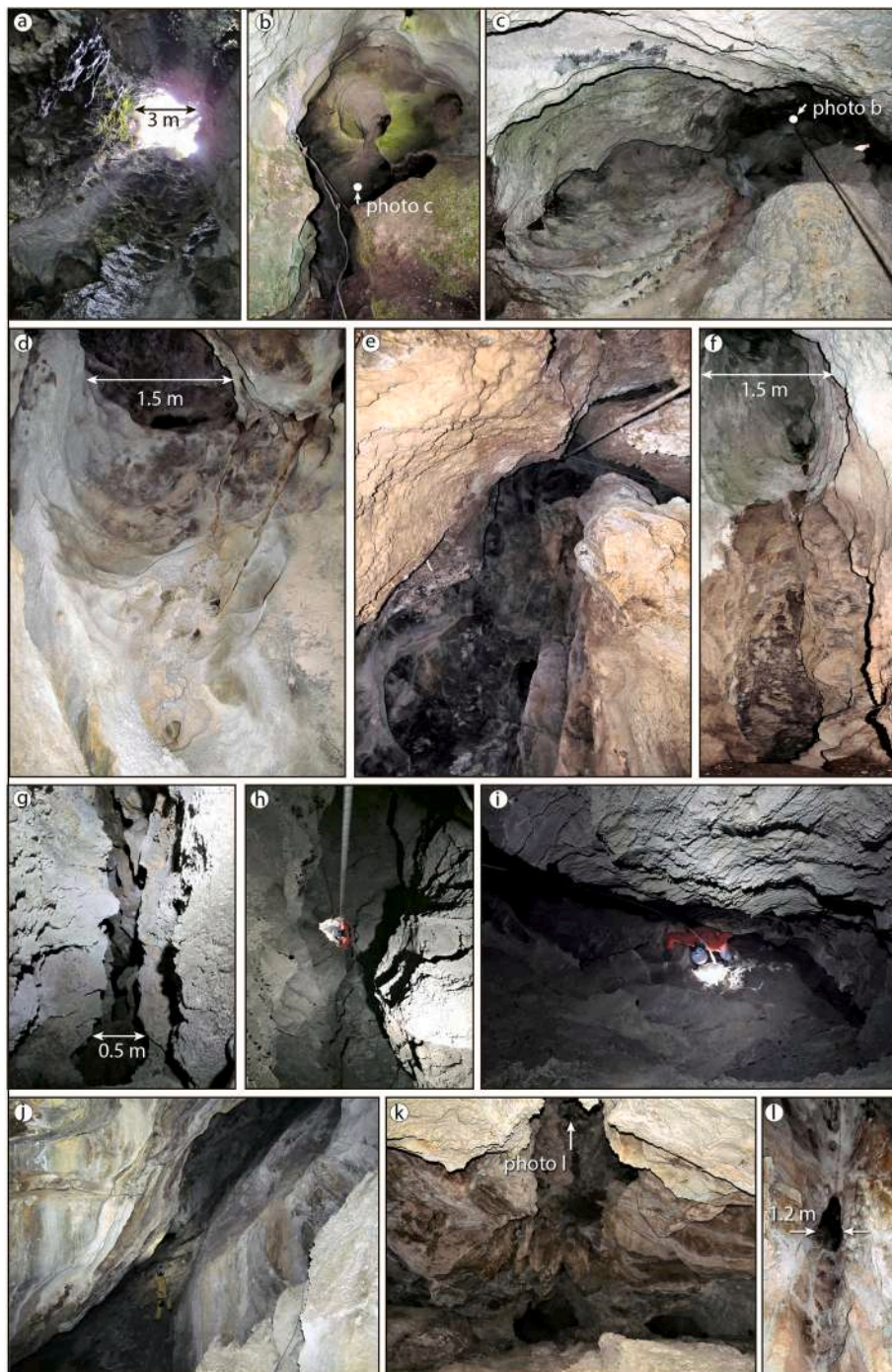


Fig. 10. Main hypogene karst structures in Tucush: a–f - rising shafts; g–i - enlarged vertical fractures (rifts); j–k - bedding-plane chambers. Photo a shows a rising shaft with solution pockets/niches and side feeders, truncated by the surface (as viewed from below). Photo b shows a «neck» of the shaft in photo c as viewed from above; c, d, e, f - top upper sections of rising shafts with ceiling convection channels and cupolas, as viewed from below; g - rift-like conduit (lateral view); h–i - rift-like conduit as viewed from above; j - bedding-plane controlled chamber (along-strike view); k - same chamber viewed up-dip, continued by three individual conduits (arrow points to a rising chimney/shaft, shown in photo l as viewed from below). Caves (see Fig. 5 for locations): a - CTU122; b, c, d, e, and f - CTU162; g, h, and i - CTU09; j, k, and l - CTU89.

produce sulfuric acid under oxygenated conditions at the water table and above it. It usually leaves clear morphological marks of the water table position. Both such conditions and the respective evidence for this process are absent; moreover, the large vertical range of the occurrence of hypogene morphs does not conform to this possibility.

Caves with rising flow features are mainly vertical shafts crossing stratigraphy, although some passages are formed along bedding planes. The resulting cave systems demonstrate a stair-case-rising geometry, somewhat similar to patterns exemplified by some hypogene caves in France (Audra, 2017) and Italy (Galdenzi and Menichetti, 2017). These systems in Tucush are documented to occur within the elevation range of at least 300 m (Fig. 13) but this diapason is likely greater as most of them continue to depth.

The only plausible explanation for the observed characteristics of caves with rising flow features is their formation by rising hydrothermal flow affecting the Tucush area. The thorough analysis of the geological settings and history of the area (Section 3) shows that the only event that could cause hydrothermal rising circulation in the Jumasha Fm was the emplacement of the nearby porphyry intrusions, dated by other studies at 9.5–11 Ma. Moreover, the porphyry stock and the study area are structurally connected via large NE-trending fractures and evidence of hydrothermal alteration of the Jumasha limestone is present in the area. We, therefore, believe that the entirety of these data and arguments provide a firm ground for a conclusion about the hypogene (hydrothermal) origin of rising flow morphologies in Tucush. This conclusion is supported by a decreasing number of caves further away from the

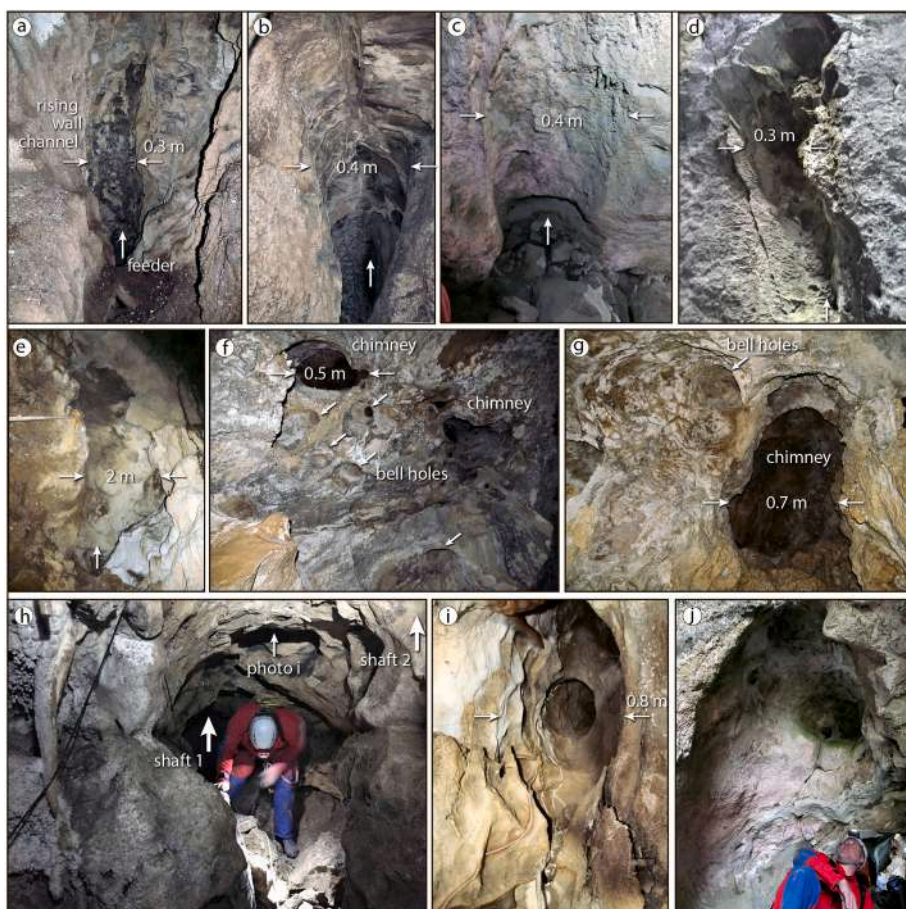


Fig. 11. Typical meso-morphological features in Tucush caves: a–e - side feeders (all but c open to shaft walls) and associated rising wall channels; f–g - ceiling features - bell holes and chimneys, as viewed from below; h - bedding-controlled passage connecting two rising shafts; i - nested cupolas in the passage in h, as viewed from below; j - nested cupolas in a bedding-controlled passage, presumably connecting two rising shafts in CTU163. Caves (see Fig. 5 for locations): a and b - CTU162; c and j - CTU163; d, e, h, and i - CTU122; f and g - CTU89.

hypogenic fluid source along the strike of the same limestone units of the Jumasha Fm.

No cave formations and minerals specific for hypogene speleogenesis have been found in the studied caves. However, the minerals which comprise assemblages in the ferruginous fill of the solutionally-widened bedding plane exposed in CTU89, and in clay sediments found in CTU112 and CTU122 caves (beidellite, siderite, opaline silica, allophane, goethite, and hematite), commonly form in hydrothermal deposits or result from the hydrothermal alteration of host rocks. Although the bedding cavity fill in CTU89 likely predates the cave formation by rising flow, its mineral composition attests with certainty to an early phase hydrothermal fluids circulation in this area. It is not clear if the mineral composition of cave clays resulted from their hydrothermal alteration in the cave environment by similar fluids during the subsequent main speleogenetic phase, or if it is the result of the redistribution of minerals eroded from the earlier bedding plane mineralization.

Epigene (vadose) shafts are also frequent in the Tucush area. In the studied caves, they are formed through the superposition of the vadose flow over relict hypogene shafts, variably modifying the latter. Most of shafts in the Tucush area, of whatever origin, have geomorphological positions discordant to the present-day landscape. Some studied vadose shafts (e.g. CTU09 and CTU165) are well-developed, large in cross-section, but clearly truncated by vigorous denudation. The same is evident for exhumed shafts and caves of hypogene origin (Fig. 6). The formation of vadose shafts is not related to the modern epikarst zone, which is generally poorly developed. This suggests that there was a major stage of epigene karstification in the past, during which time a more mature karst landscape once existed. The mature karstic surface and the epikarst zone were later removed by glacial scouring during the LGM. The major stage of epigene karstification likely occurred earlier than the incision (deepening) of the upper stretch of the Ayash Valley;

hence the karst system development may have been controlled by another base-level.

Development of vertical conduits (shafts) in the vadose zone is not controlled nor diverted by marly interbeds, as evidenced by shafts cutting across marl layers. The presence of open throughgoing fractures of the NE orientation and pre-formed hypogene shafts along them allows for turbulent flow and considerable erosion in the modern vadose conditions so that difference in the purity and solubility of the different carbonate layers does not play a major role in the development of vertical conduits. Moreover, the presence of considerable pre-formed hypogene cave porosity at depth provides the space to accommodate residual clay released by dissolution and erosion of marly beds, preventing blockage of groundwater flowpaths in the zone of active circulation. Deeper (regional) circulation, however, is likely to be hampered in the modern hydrogeological system.

7.2. Evolution of karst

7.2.1. Hypogene karstification

Hypogene karst void/conduit systems in the Antamina/Tucush area are strongly controlled by geologic structure and demonstrate a high degree of morphological integrity. Their formation clearly post-dates the main deformation periods during which the regional thrust-fold structure and major tectonic discontinuities were formed.

The analysis of geological and geodynamic history of the region discussed in Sections 2 and 3 strongly suggests that hypogene karstification in the area is related to a hydrothermal system associated with the emplacement of the nearby porphyry intrusions and the formation of the Antamina deposit (Fig. 14). The intrusion emplacement was strongly controlled by the NE-trending Valley Fault System (Love et al., 2004; Mrozek, 2018). Studies demonstrate that various fluid-



Fig. 12. Vadoso overprint over hypogene morphologies in Tucush caves: a and b - vadoso shaft cutting through hypogene cavities; c - vadoso shaft breaching into a hypogene chamber; d and e - vadoso overprint (dissolution and deposition) over hypogene shafts (note the remnant of a hypogene rising channel and a chimney in the upper right part of e); f and g - vadoso meanders; h - vadoso cutting in the floor of a bedding-controlled hypogene chamber (shown in Fig. 9 j). Caves (see Fig. 5 for locations): a and b - CTU09; c - CTU166; d and g - CTU122; e and h - CTU-89; f - CTU162.

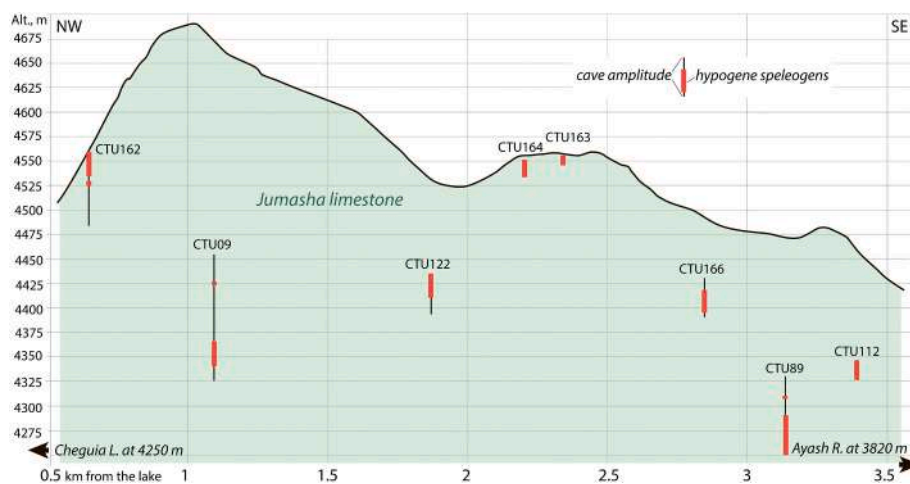


Fig. 13. Profile along the crest of the Tucush ridge showing distribution of rising flow features sections in the studied caves (projected onto the profile).

induced alterations of the host rocks extend up to a few kilometers around the intrusion boundaries, being predominantly guided by NE-trending fractures (Love et al., 2004; Escalante, 2008; Escalante et al., 2010). Hypogene karstification in the Tucush area, which lies immediately NE of the Antamina porphyry center (Fig. 5), clearly resulted by the transport of aggressive hydrothermal fluids from the intrusion along these NE oriented fractures. Hypogene karst in the Antamina/Tucush area would therefore be classified as endogenous type of hypogene

karstification (Klimchouk, 2017).

Skarn deposits form when magmas, intruded into carbonate-rich host rocks, generate a hydrothermal system involving magmatic and metamorphic fluids. Models for the genesis of giant porphyry Cu systems in the central Andean orogen postulate rapid ascent of magma (Love et al., 2004) with high magmatic water contents (Mrozek, 2018). When the magma reaches the shallow crust, changes in pressure and temperature allow the volatiles to rapidly escape, sometimes in an explosive manner.

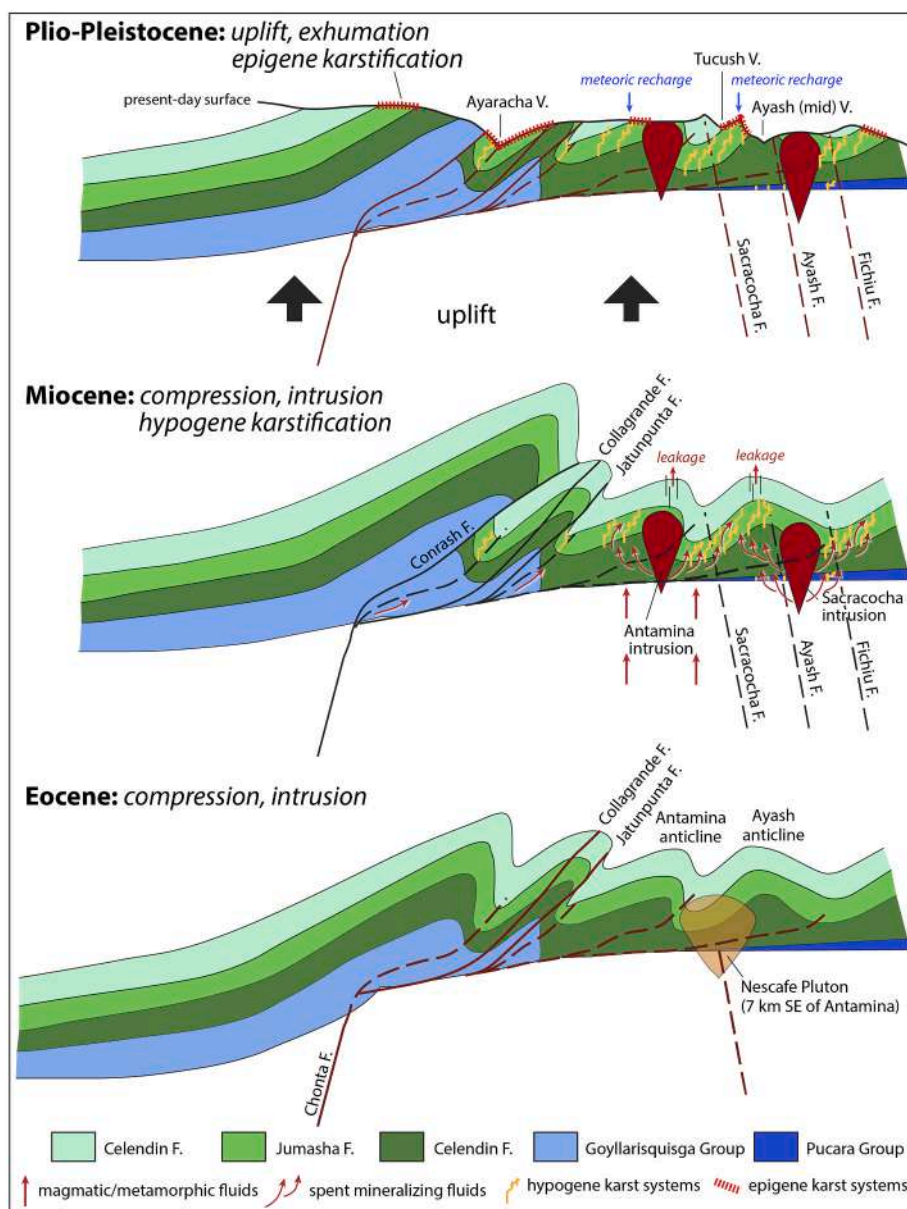


Fig. 14. Hypogene karstification in the Antamina area in the context of regional geodynamic evolution (structural pattern is adopted from BISA Technical Report, 2015).

The main volatiles are water vapor and CO₂, but other gases such as HCl, SO₂, H₂S, HF, H₂, and CO are also common (Fischer and Chiodini, 2015). These highly aggressive acidic fluids periodically released from the porphyry center over a long period of time (roughly 1.5 Ma; Mrozek, 2018) provided ample potential for dissolution of the host country rocks, particularly carbonates. In addition, large amount of CO₂ and carbonic acid is produced during the skarn formation, further enhancing the aggressiveness of the fluids.

Love et al. (2004) infer the formation of skarn and metamorphism of limestone at ca. 495 °C. Based on the study of fluid inclusions in comb-layered quartz, the earliest fluids that exsolved directly from magma in the Antamina porphyry center were characterized by salinity ranging from 46.7 to 52.3 wt% NaCl equiv., density in a range of 1.1 to 1.2 g/cm³, pressures in a range of 0.95 to 1.2 kbar, and temperatures in a range of 405 °C to 420 °C (Mrozek, 2018). Based on these pressures, Mrozek (2018) estimated a maximum formation depth for the top of the Antamina porphyry center ranging from 4.6 to 3.5 km (averaging 4.1 km).

Recent studies constrained the duration of magmatic-hydrothermal

activity at Antamina to ca. 1.5 Ma roughly between 11 Ma and 9.5 Ma (Mrozek et al., 2015, 2017; Mrozek, 2018). These studies distinguished three major intrusive phases and at least eleven sub-phases at Antamina, based on cross-cutting relationships of main intrusive centers and various sub-bodies (dikes, veins, etc.). Love et al. (2004) envisaged that the Celendín Formation hornfels capped the ore-forming system at Antamina, promoting recirculation of hydrothermal fluids and extensive endoskarn development. In areas away from the hornfels cap, the Celendín Formation, although being generally a seal for the hydrothermal reservoir, was locally leaky along tectonic discontinuities, which promoted escape of spent fluids (i.e. hydrothermal fluids that lost part of the originally carried elements) away from the main intrusive stock. The escape pathways northeast of the intrusive complex were mainly NE-trending major throughgoing fractures (sensu Gross and Eyal, 2007). Escaping fluids followed these discontinuities, and locally bed-confined joints of the same direction and bedding planes connecting the major throughgoing fractures where they were vertically and laterally offset relative to each other. The resulting cave systems therefore have a stair-

case-rising geometry. In the plan view, individual hypogene cave systems occurred through the area as NE-elongated clusters, which were largely isolated from each other along the formation strike (Fig. 15a).

We do not have many clues to infer about the chemical-physical attributes of spent fluids that circulated through the Jumasha limestones in the Tucush area and formed rising cave systems. It can be expected that fluids escaping the intrusion and skarn at high-sulfidation deposits are to be low-pH due to condensation of oxidized HCl- and SO₂-rich vapor (Dilles and John, 2021), and CO₂-enriched due to the contact decarbonation. The fluid attributes and escape flow dynamics were likely changing considerably during the multiphase history of the magmatic-hydrothermal activity of the Antamina region. It can be supposed that hypogene speleogenesis was related to some of the later phases, when spent fluids increasingly escaped the skarn around the

Antamina intrusive stock and flowed outward and upward through the Jumasha limestone in the Tucush area, according to the structural guidance by the NE-trending fractures. Temperatures at the distance of 1.5–3 km from the stock probably did not exceed 180–200 °C, based on the mineral assemblages in the fill of the solutionally-widened bedding plane in CTU89 and in clay sediments found in CTU112 and CTU122 caves, decreasing progressively outward and upward.

As CO₂-rich fluids move away from the intrusion zone and skarn and dissolve limestones, their dissolution capacity is renewed along the flowpaths due to the retrograde solubility of calcite, which enables karstification by cooling of upward flowing waters. In the Antamina area, cooling during the fluid ascent is recorded by the oxygen isotopic enrichment of calcite in veins and their wallrocks with increasing elevation (Escalante, 2008). Carbonic acid dissolution by hydrothermal fluids due to the retrograde solubility of calcite can, therefore, be inferred as the most likely chemical mechanism of hypogene karstification in the area, although other acids could also be involved.

Chaudhuri et al. (2013) simulated hypogene karstification by rising and cooling hydrothermal flow in a 900 m high vertical fracture in a mountain hydrologic system using a coupled thermohydrochemical model which considers both calcite dissolution kinetics and buoyancy effects. They demonstrated the development of high-permeability sub-vertical conduits in the conductive heat transfer regime and the expressive effects of buoyant convection, including the formation of features of the “morphological suite of rising flow” described by Klimchouk (2009a). They also noted that along the rising thermal flow conduits, retrograde solubility and mixing corrosion effects could combine to produce favorable conditions for karstification. These modeling results illustrate a likely mechanism of hypogene speleogenesis in the Tucush area. Additional mineralogical and geochemical studies of cave formations and sediments, and particularly studies of the stable isotope imprint in the cave walls (e.g. Dublyansky et al., 2014; Spötl et al., 2021), are needed to shed more light on physical-chemical conditions and specific processes of hypogene karstification in the area.

Magmatism in the region ceased by 6.3 Ma (Love et al., 2004), with moderate to rapid post-intrusive cooling in the Miocene (Garver et al., 2005). The specific history of cooling and depressurization of the hydrothermal reservoir probably accounts for the absence of substantial mineral deposition in hypogene caves in Tucush. Subsequent events such as uplift, exhumation, and denudation shifted hypogene caves from their native deep settings to shallow environments (Fig. 14 upper). Upon the removal of the Celendín Formation and exposure of the Jumasha limestones over much of the Tucush area, epigene karstification commenced.

7.2.2. Epigene karstification

7.2.2.1. Pre-LGM phase. Rapid and continuous exhumation of the region through both erosional and tectonic processes has occurred since 5–6 Ma, with total unroofing during the latest phase (the Cañon stage of erosion) estimated at 4.5–5 km (Perry and Garver, 2004; Garver et al., 2005). Assuming the thickness of the removed cover over the Jumasha Formation at 4 km, and the denudation rate at 1.5 mm/year (Garver and Rodbell, 2002), the Jumasha limestones in the Antamina/Tucush area began to be exposed around 2.6 Ma, i.e. at the Pliocene/Pleistocene cutoff. Since then, epigene karstification commenced in the area and developed with varying intensity determined by climate and neotectonic/geomorphological factors. It is likely that an extensive karst landscape with a thick and mature epikarst zone and considerable conduit systems developed during the Early and Middle Pleistocene. Mature large vadose shafts with truncated “heads”, found in the Tucush area, clearly pre-date at least the LGM. The intense epigene karstification in the end of the Early Pleistocene is supported by age dating of the massive vadose flowstone found in CTU122 cave at >700 ka.

Epigene karst development was strongly influenced by the inherited

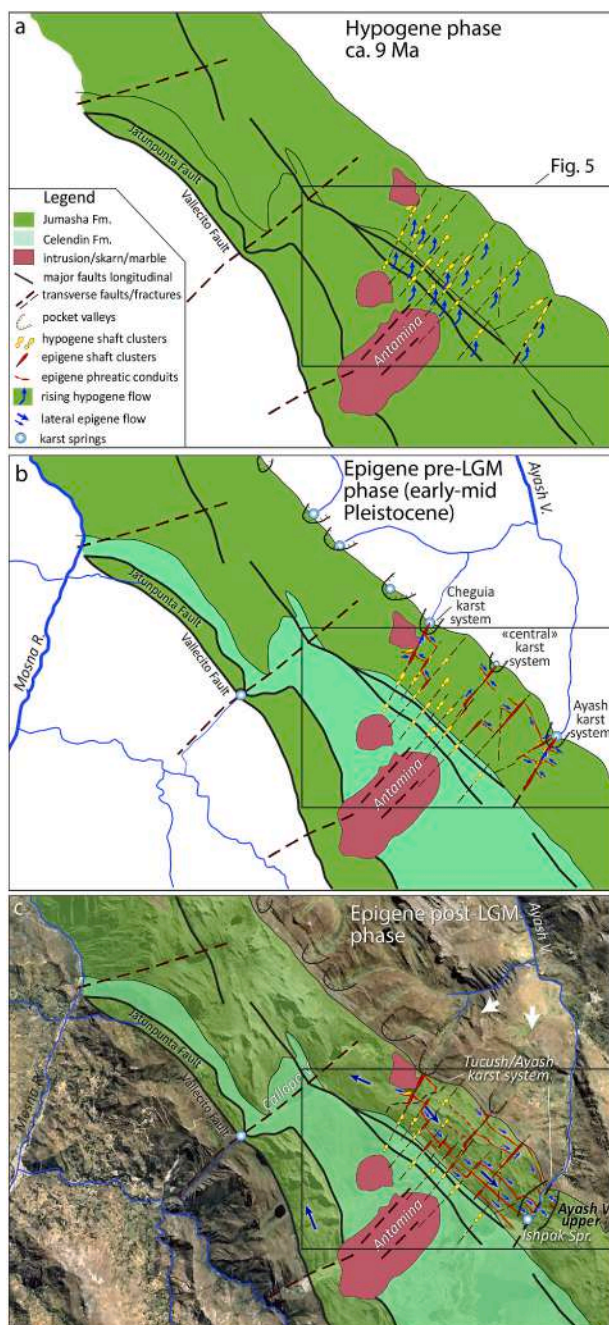


Fig. 15. Evolution of karst in the Tucush area, showing hypogene (a), epigene pre-LGM (b), and epigene post-LGM (c) phases.

hypogene karst structures comprising stair-case-rising shaft systems. We recognize several interrelated effects that the presence of these structures imposed on subsequent epigene karstification. They provided pre-formed, effective vertical drains across the vadose zone, thus facilitating rapid deepening of the vadose zone, depending on the outflow conditions. These shafts occasionally (locally) opened through geomorphological interception to receive surface recharge either directly or through epikarst. The outflow conditions depended on the availability of high-permeability structures in the phreatic zone and on hydraulic gradients. These conditions greatly varied between localities and through time. Thus, the pre-existing sub-vertical hypogene shaft systems determined a complex pattern of hydraulic compartments, which interplay influenced the initiation and development of lateral phreatic conduits. As hypogene caves in Tucush are strongly controlled by the NE-trending fractures, the development of epigene phreatic conduits along these fractures was favored. However, strike-parallel conduit development in the phreatic zone was less favored during this phase, being dependent on gradients between adjacent compartments and the availability of respective connecting preferential flow paths.

The potential for epigene karstification highly depended on the position and depth of the draining base-level. It is apparent that the upper Ayash canyon, which presently drains the Tucush karst system, did not exist before the Last Glacial Period (i.e. before ca. 120 Ka) and likely before the LGM. The head of the present-day Ayash Valley is located at the confluence of the Tucush and Huincush valleys, both hosting large glaciers during the LGM. This is evidenced by clear signs of glacial erosion and the presence of glacial deposits in both valleys. If the upper Ayash Valley existed at the time of the LGM, it would have served as a major outlet for the ice from the Tucush-Huincush glaciers and, accordingly, the Ayash Valley would be U-shaped (similarly to the Antamina and Callapo valleys). However, the upper Ayash Valley is V-shaped and its lower slopes are devoid of appreciable signs of glacial erosion.

There are two possible scenarios regarding which base-level controlled epigene karstification during most of the Pleistocene (Fig. 16a). One is the Mosna-Puchca Valley, which deeply cuts the Jumasha limestone belt in two stretches located 13.5 and 15 km NW of the Tucush area. The Mosna-Puchca scenario (brown arrows in Fig. 16a) implies deep sub-regional flow in the strike-parallel direction along the limestone belt. However, the presence of large transverse faults and related incised valleys (e.g. Callapo Valley) could intercept and divert groundwater flow to the western boundary of the Jumasha Fm.

Another base-level scenario is related to the middle stretch of the Ayash Valley (blue arrows in Fig. 16a; the middle Ayash scenario), which may have been deep enough during the Pleistocene to drain the surrounding formations. Jumasha Formation drainage in the NE direction would have been greatly favored by the presence of the transverse (NE-trending) open fractures and hypogene systems controlled by them (Fig. 15b). Drainage from the NE-oriented transverse karst systems, however, would have been dammed by the Pariatambo Formation (Ki-Pa; non-karsifiable Cretaceous rocks), which forms the NE contact with the Jumasha Formation. This contact outcropped at significantly lower altitudes than those along the bottom of the intramountainous Tucush Valley before the latter had been deepened by glacial erosion during the LGM. The elevations of these contacts were low enough to provide sufficient gradient to drive the flow in the NE direction. These altitudes, however, were significantly higher than the altitudes at the middle Ayash stretch so that the Ki-Ju1/Ki-Pa contact formed the barrier causing the overflow conditions. The occurrence of focused discharge along the NE boundary of the Jumasha limestones in the past is corroborated by the presence of a series of pocket-headed valleys located along the contact (Fig. 16).

Based on the location of the valleys along the NE slope of the Tucush ridge (possibly indicating major points of karstic discharge), at least three large, parallel, transverse karst systems are inferred to operate there during the pre-glacial phase: the Cheguia, "Central", and Ayash

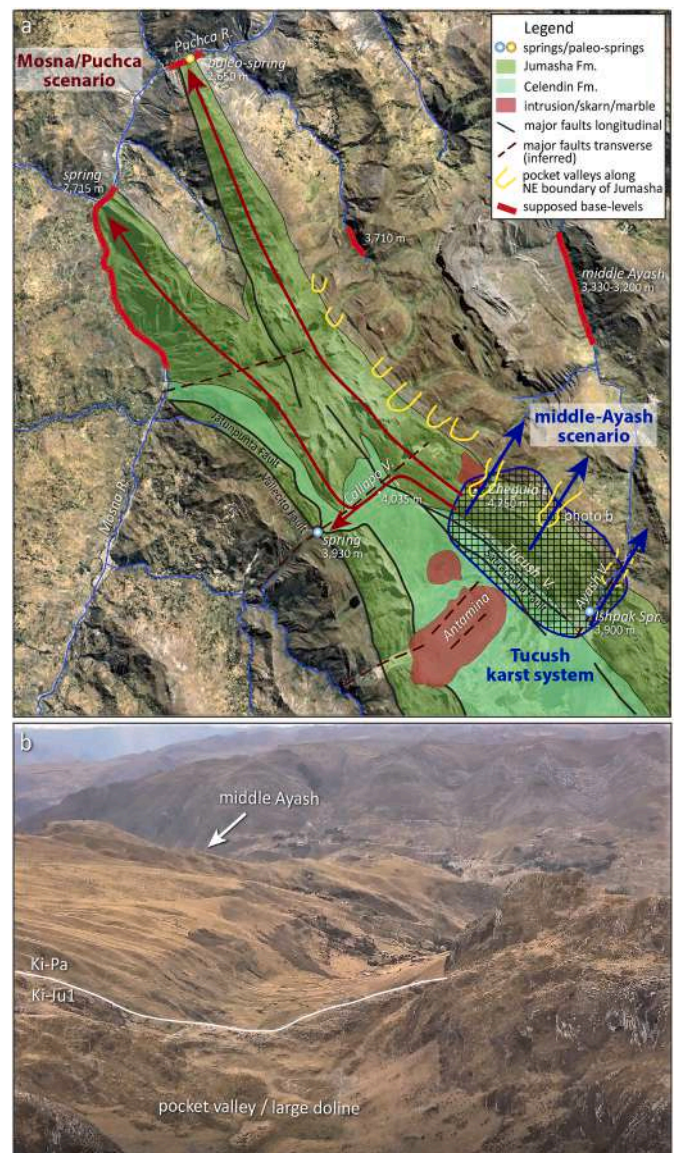


Fig. 16. Two scenarios of the base-level control of the Tucush karst during the main (pre-LGM) phase of epigene karstification (a) and an oblique drone view of a NE-stretching pocket valley which starts near the Ki-Ju1/Ki-Pa contact (b).

systems (Fig. 16a). At the water-table and phreatic zone levels, these systems likely consisted of major trunk passages integrating pre-existing hypogene caves along prominent NE discontinuities, and secondary tributary conduits formed along strike-parallel discontinuities due to the drainage of the adjacent blocks of the Jumasha limestones.

7.2.2.2. The role of glaciations. The timing and the relative geomorphic roles of various phases of Pleistocene glaciations are not well constrained for this part of Andes. Evidence from the wider region, such as dated at >400 ka moraines down-valley of the LGM moraines (Farber et al., 2005), indicate that the maximum ice volumes and extent of glaciers predate the LGM. Studies also show a consistent pattern of an early LGM advance (34–27 ka; Clapperton, 1998), followed by late glacial advance, and rapid deglaciation by ~20 ka (Zech et al., 2009; Mark et al., 2017).

Pleistocene glaciations, particularly the LGM, have greatly contributed to the geomorphological evolution of the Antamina/Tucush area and exerted considerable impact on karst development. The Tucush and Huincush valleys, which bottoms are now covered by waste rocks and

tailings, respectively, have accommodated significant glaciers during the Middle and Late Pleistocene, and their upper slopes display numerous smaller glacial-shaped valleys and cirques that fed the main glaciers. During the progressive phase of glaciations, karst development is hindered since the ice cover reduces the amount of recharge into the karst system. As well, glacial scouring can remove the pre-existing epikarstic zone and decapitate/unroof shafts and caves (Klimchouk et al., 2006; Audra et al., 2007). These effects are clearly observable in the Tucush area and include scoured epikarst, decapitated vadose shafts, and unroofed hypogene cavities.

In warm-based glaciers, liquid water coexists with glacier ice so karst may continue to develop even during glaciations although recharge to the underlying rocks is more focused according to the interplay of glacial hydrology and the basement topography. The regressive phase of glaciations provides significant and largely focused recharge to the underlying karst aquifer. Glaciers resting on karstified limestones may develop large closed and semi-closed basins due to both, their erosive action and focused underground drainage of melt waters. Large dolines in the Tucush ridge likely owe their origin to glaciations.

The major underground drain for the melt water during the deglaciation was at the confluence of the Tucush and Huincush valleys, where the well-developed transverse Ayash karst system likely presumably existed in the place of the current Ayash canyon (Fig. 15b). The Ayash valley in that time was likely a shallower, pocket-headed valley on the NE side of the Tucush ridge, not connected upstream to the Tucush-Huincush glaciers/valleys, i.e. not cutting through the entire limestone strip. This scenario is analogous to the present-day Laguna Cheguia basin situated northwest of the Ayash Valley, which only partly entrenches the Tucush Ridge (see Fig. 3). Highly focused, massive development of the Ayash karst system during the glacial decay facilitated its subsequent unroofing and rapid formation of the Ayash canyon, breaching upstream to the Tucush-Huincush confluence. Hence, the upper Ayash valley could have formed during the last massive deglaciation around 20 ka, establishing a new base-level for karst development.

7.2.2.3. Post-LGM (contemporary) phase. The contemporary karst development is strongly influenced by pre-formed caves, either hypogene and those formed during the pre-LGM phase of epigene karstification.

The epikarst zone is redeveloping after the last glacial scour but is still immature and has a limited capacity of retaining groundwater and regulating recharge. The redevelopment of epikarst is somewhat hampered by the presence of pre-formed shafts capable of effectively transferring recharge across the vadose zone. It occurs under a combined control of transverse discontinuities and pre-formed caves/shafts, strike-parallel structures, and lithological variations across the strike. Surface karst landforms are dominated by features forming through adaptation of exhumed/unroofed elements of pre-existing caves. Interception by the denudation surface of hypogene shafts creates sinkhole-like features. Where the surface unroofs rift-like or bed-parallel conduits, prominent transverse surface corridors develop. Representative examples are CTU163 and CTU164 caves (Figs. 12 and 13).

The establishment of the upper Ayash canyon across the Jumasha Formation at the end of LGM radically changed the groundwater flow system in the Tucush area. This new base-level has been gaining increasing control over karstification, facilitating the development of strike-parallel conduits in the phreatic zone. The pre-formed transverse karst structures become increasingly integrated by such conduits, although they still determine some degree of aquifer compartmentalization along the formation strike, which is corroborated by the piezometric data from boreholes and hydrograph data from the Ishpac Spring. The zone of the hydraulic influence of the upper Ayash canyon has advanced along the strike as far as the immediate vicinity of the Cheguia Lake, which is evidenced by the dye tracing connection between CTU162 cave to the Ishpac Spring.

Dye tracing studies to the date have revealed the existence of at least two strike-parallel conduit systems separated by the marly Sucesión Marcadora (Ks-Ju2sm), - one in the Ks-Ju2 unit (the most karstified unit of the Tucush Ridge) and the other in the Ks-Ju3 unit. Although the Succession Marcadora causes substantial compartmentalization in the transverse direction, hydraulic connection across it, however, locally occurs via transverse discontinuities and associated shafts.

8. Conclusions

The karst system in the Antamina/Tucush area has formed as the result of polygenetic and multi-phase karst development. It is a complex mix of solution void and conduit components of different origins formed in multiple stages, variously integrated into the modern groundwater flow system. At least three major phases of karstification are identified (from the oldest to the youngest): (1) hypogene karstification; (2) major epigene karstification, likely controlled by the barrier of insoluble formations along the NE boundary of the Jumasha limestones; and (3) contemporary epigene karstification controlled by the upper Ayash canyon.

Hypogene karstification in the Antamina/Tucush area is related to a hydrothermal system associated with the same magmatic event that was responsible for the emplacement of the nearby porphyry intrusions and the formation of the Antamina deposit, the world's largest known copper-zinc skarn ore deposit. Dissolution by hypogenic fluids released from the intrusive events resulted in the formation of deep-rooted, laterally isolated stair-case-rising shaft systems aligned along transverse (NE-trending) cross-formational fractures. The studied hypogene caves stand as a foremost example of endogenous hypogene speleogenesis related to magmatic intrusions. They clearly exhibit a complete suite of speleogens indicating rising flow and are remarkably well-preserved, despite the long time elapsed since their formation (ca. 9–10 Ma). The most likely chemical mechanism of hypogene karstification in the area is carbonic acid dissolution by rising and cooling hydrothermal fluids due to the retrograde solubility of calcite, although other acids and mixing corrosion effects could also be involved. Epigene karst development was strongly influenced by the pre-existing hypogene karst structures as the latter provided effective vertical drains across the vadose zone. Hypogene conduits, however, were only discretely utilized by the unconfined groundwater circulation. The overprint of epigenic features over hypogene morphologies is very distinct and easily recognizable. Moreover, the transverse discontinuities and linear series of hypogene caves aligned to them favored the development of epigene phreatic conduits across the ridge, likely toward the contact barrier and ultimately the middle Ayash. Several largely independent, sub-parallel transverse karst systems are inferred to have developed in the Tucush area during the second phase, including the one that became a precursor for the later formation of the Ayash canyon.

The third phase commenced with the establishment of the upper Ayash canyon across the Jumasha limestone belt at the end of LGM, which re-oriented the groundwater flow in the Tucush area. This new base-level facilitated the development of strike-parallel conduits in the phreatic zone toward the upper Ayash and ongoing integration of the previously independent transverse karst systems. This process extended the hydraulic influence of the Ayash canyon at least 4 km NW (along the formation strike), although certain degree of aquifer compartmentalization in this direction still remains.

The polygenetic and multi-phase nature of the Tucush karst system is the main cause for the complexity of the hydrogeologic system in terms of its hydraulic structure and functioning. This study suggests that the inheritance of hypogene karst features can be a major factor influencing contemporary karstification at ore deposits located in carbonate terrains. It also illustrates that understanding of the origin and evolution of karst is crucial for development of sound conceptual groundwater flow models for karst terrains, as well as for the assessment of karst-related hazards and risks.

Declaration of competing interest

The authors declare the following financial interests/personal relationships which may be considered as potential competing interests: Alexander Klimchouk, David Evans, Sasa Milanovic, Cristian Bittencourt, Mauro Sanchez, Carlos Aguirre F. report financial support was provided by Minera Antamina. Mauro Sanchez, Carlos Aguirre F. report a relationship with Minera Antamina that includes: employment. David Evans reports a relationship with FloSolutions that includes: board membership and employment. Alexander Klimchouk, Sasa Milanovic, Cristian Bittencourt reports a relationship with FloSolutions that includes: consulting or advisory.

Data availability

Relevant research data are contained in the paper

Acknowledgements

We thank the Minera Antamina for initiating and funding this study and for granting permission for this publication. We also thank Gary Olivo from Antamina and cavers Julio Maguina, Carlos Pizarro, and Ernesto Dueñas for their technical support in the speleological work. We are grateful to the reviewers, Prof. Jo De Waele and Dr. Philippe Audra for their constructive comments that allowed improving the original manuscript. Prof. Hai Cheng and Dr. Yury Dublyansky are thanked for dating of a flowstone sample. Preparation of the paper was partially supported by the NAS of Ukraine through the project “Resource and geocological aspects of anomalous hydrogeological processes and conditions”.

Appendix A. Supplementary data

Supplementary data to this article can be found online at <https://doi.org/10.1016/j.geomorph.2022.108488>.

References

- Antamina Technical Report, 2015. El Karst de Antamina.
- Apaza-Idme, D., Pulido-Bosch, A., Sánchez-Martos, F., Recursos, G.I., 2015. Karstic hydrogeology of the Uchucchacua underground mine (Perú) and its interaction with surface waters. In: Andreo, B. (Ed.), *Hydrogeological and Environmental Investigations in Karst Systems*, Environmental Earth Sciences, 1. Springer-Verlag, Berlin Heidelberg, pp. 477–485. https://doi.org/10.1007/978-3-642-17435-3_54.
- Audra, P., 2017. Hypogene caves in France. In: Klimchouk, A., De Waele, J., Palmer, A. N., Auler, A.S., Audra, P. (Eds.), *Hypogene Karst Regions and Caves of the World*. Springer International Publishing AG, Cham, pp. 61–83.
- Audra, P., Mocochain, L., Camus, H., Gilli, E., Clauzon, G., Bigot, J.-Y., 2004. The effect of the Messinian deep stage on karst development around the Mediterranean Sea. *Examples from southern France*. *Geodin. Acta* 17 (6), 27–38.
- Audra, P., Mocochain, L., Bigot, J.Y., Nobécourt, J.C., 2009a. Morphological indicators of speleogenesis: hypogenic speleogens. In: Klimchouk, A., Ford, D. (Eds.), *Hypogene Speleogenesis and Karst Hydrogeology of Artesian Basins*. Ukrainian Institute of Speleology and Karstology, Simferopol, pp. 17–22.
- Audra, P., Mocochain, L., Bigot, J.Y., Nobécourt, J.C., 2009b. Hypogene cave patterns. In: Klimchouk, A.B., Ford, D.C. (Eds.), *Hypogene Speleogenesis and Karst Hydrogeology of Artesian Basins*. Ukrainian Institute of Speleology and Karstology, Simferopol, pp. 23–32.
- Audra, Ph., Bini, A., Gabrovšek, F., Häuselmann, Ph., Hobléa, F., Jeannin, P.-Y., Kunaver, J., Monbaron, M., Süsteršič, F., Tognini, P., 2007. Cave and karst evolution in the Alps and their relation to paleoclimate and paleotopography. *Acta Carsologica* 36 (1), 1580–2612. <https://ojs.zrc-sazu.si/carsologica/article/view/208>.
- Bauer, S., Liedl, R., Sauter, M., 2005. Modeling the influence of epikarst evolution on karst aquifer genesis: a time-variant recharge boundary condition for joint karst-epikarst development. *Water Resour. Res.* 41, W09416 <https://doi.org/10.1029/2004WR003321>.
- BISA Technical Report, 2015. Actualization de low modelos geologicos estructurales del distrito minero de Antamina.
- Bissig, T., Tosdal, R., 2009. Petrogenetic and metallogenetic relationships in the Eastern Cordillera Occidental of Central Peru. *J. Geol.* 117 (5), 499–518. <https://doi.org/10.1086/600862>.
- Bodenlos, A.J., Erickson, G.E., 1955. Lead-zinc deposits of Cordillera Blanca and northern Cordillera Huayhuash, Peru. In: *United States Geological Survey Bulletin*, 1017.
- Bonnot, D., Sebrier, M., Mercier, J., 1988. Evolution géodynamique plio-quaternaire du bassin intra-cordillèrain du Callejon de Huaylas et de la Cordillère Blanca, Pérou. *Géodynamique* 3, 57–83.
- Chaudhuri, A., Rajaram, H., Wiswanathan, H., 2013. Early-stage hypogene karstification in a mountain hydrologic system: A coupled thermohydrochemical model incorporating buoyant convection. *Water Resour. Res.* 49, 5880–5899. <https://doi.org/10.1002/wrcr.20427>.
- Clapperton, C.M., 1998. Late Quaternary glacier fluctuations in the Andes: testing the synchrony of global change. *J. Quat. Sci.* 6, 65–73.
- Cobbing, E.J., Pitcher, W.S., Wilson, J.J., Baldock, J.W., Taylor, W.P., McCourt, W.J., Snelling, N.J., 1981. *The Geology of the Western Cordillera of Northern Peru*. Overseas Memoir of the Institute of Geological Science London, Memoir, 5, 143 p.
- De Waele, J., Gutierrez, F., 2022. *Karst Hydrogeology, Geomorphology and Caves*. John Wiley & Sons.
- Dilles, J.H., John, D.A., 2021. Porphyry and epithermal mineral deposits. In: Alderton, D., Elias, S.A. (Eds.), *Encyclopedia of Geology*, 2nd edition. Elsevier, pp. 847–866. <https://doi.org/10.1016/B978-0-08-102908-4.00005-9>.
- Dublyansky, Y.V., Klimchouk, A.B., Spöt, C., Timokhina, E.I., Amelichev, G.N., 2014. Isotope wallrock alteration associated with hypogene karst of the Crimean Piedmont, Ukraine. *Chem. Geol.* 377, 31–44.
- Escalante, A., 2008. Patterns of distal alteration zonation around Antamina Cu–Zn Skarn and Uchucchacua Ag–basemetal vein deposits, Peru. Unpublished PhD dissertation. In: *Mineralogical, Chemical and Isotopic Evidence for Fluid Composition, and Infiltration, and Implication for Mineral Exploration*. The University of British Columbia. <http://hdl.handle.net/2429/154>.
- Escalante, A., Dipple, G.M., Barker, S.L.L., Tosdal, R., 2010. Defining trace-element alteration halos to skarn deposits hosted in heterogeneous carbonate rocks: Case study from the Cu–Zn Antamina skarn deposit, Peru. *J. Geochem. Explor.* 105, 117–136.
- Evans, D., 2015. Hydrogeological risks of mining in mountainous Karstic Terrain: lessons learned in the Peruvian Andes. In: Andreo, B. (Ed.), *Hydrogeological and Environmental Investigations in Karst Systems*, Environmental Earth Sciences, 1. Springer-Verlag, Berlin Heidelberg, pp. 465–475. https://doi.org/10.1007/978-3-642-17435-3_53.
- Evans, D., Waltham, T., 2022. In: *Karst Geohazards. Tailings Management Handbook: A Life-Cycle Approach*. Society for Mining, Metallurgy & Exploration (SME), pp. 421–440, 143 p.
- Evans, D., Letient, H., Aley, T., 2005. Aquifer vulnerability mapping in karstic terrain—Antamina Mine, Peru. In: *Proceedings From the Society of Mining Engineers Conference, 2005 Salt Lake City, USA*, pp. 1–13.
- Farber, D.L., Hancock, G.S., Finkel, R.C., Rodbell, D.T., 2005. The age and extent of tropical alpine glaciations in the Cordillera Blanca, Peru. *J. Quat. Sci.* 20, 759–776.
- Fischer, T.P., Chiodini, G., 2015. Volcanic, magmatic and hydrothermal gases. Chapter 45. In: Sigurdsson, H. (Ed.), *The Encyclopedia of Volcanoes*, Second edition. Academic Press, pp. 779–797. <https://doi.org/10.1016/B978-0-12-385938-9.00045-6>.
- Ford, D.C., Williams, P.W., 2007. *Karst Hydrogeology and Geomorphology*. Wiley and Sons, Chichester.
- Galdenzi, S., Menichetti, M., 2017. Hypogenic caves in the Apennine Mountains (Italy). In: Klimchouk, A., De Waele, J., Palmer, A.N., Auler, A.S., Audra, P. (Eds.), *Hypogene Karst Regions and Caves of the World*. Springer International Publishing AG, Cham, pp. 127–142.
- Garreaud, R.D., Vuille, M., Compagnucci, R., Marengo, J., 2009. Present-day south American climate. *Palaeogeogr. Palaeoclimatol. Palaeoecol.* 281 (3–4), 180–195. <https://doi.org/10.1016/j.palaeo.2007.10.032>.
- Garver, J.I., Rodbell, D.T., 2002. Fission-track evidence for rapid tectonic exhumation of the Cordillera Blanca, Peru. In: *Geological Society of America, Annual Meeting, Abstracts with Programs*, 34, p. 376.
- Garver, J.I., Reiners, P.W., Walker, L.J., Ramage, J.M., Perryett, S.E., 2005. Implications for timing of Andean uplift from thermal resetting of radiation-damaged zircon in the Cordillera Huayhuash, Northern Peru. *J. Geol.* 113, 117–138.
- Glencore, 2015. Annual report. http://www.glencore.com/assets/investor/doc/reports_and_results/2015/GLEN-2015-Annual-Report.pdf.
- Gross, M., Eyal, Y., 2007. Throughgoing fractures in layered carbonate rocks. *GSA Bull.* 119 (11–12), 1387–1404.
- Guyot, J.L., Apaestegui, J., Bermudez, S., Bigot, J.Y., 2014. Un nouveau point Sur la spéléologie au Pérou. *Spelunca* 133, 1–5.
- Hall, S.R., Farber, D.L., Ramage, J.M., Rodbell, D.T., Finkel, R.C., Smith, J.A., Mark, B.G., Kassel, C., 2009. Geochronology of Quaternary glaciations from the tropical Cordillera Huayhuash, Peru. *Quat. Sci. Rev.* 28 (25–26), 2991–3009.
- Itasca Technical Report, 2003. Tucush Valley Hydrogeology Study.
- Klimchouk, A., Bayari, C.S., Nazik, L., Törk, K., 2006. Glacial destruction of cave systems in high mountains, with special reference to the Aladağlar massif, Central Taurids, Turkey. *Acta Carsologica* 35 (2), 111–122.
- Klimchouk, A., Palmer, A.N., De Waele, J., Auler, A.S., Audra, P., 2017. Hypogene Karst Regions and Caves of the World. Springer International Publishing AG, Cham. <https://doi.org/10.1007/978-3-319-53348-3>.
- Klimchouk, A.B., 2004. Towards defining, delimiting and classifying epikarst: its origin, processes and variants of geomorphic evolution. In: Jones, W.K., Culver, D.C., Herman, J. (Eds.), *Epikarst*. Karst Water Institute Special Publication 9, Shepherdstown, West Virginia, pp. 23–35.
- Klimchouk, A.B., 2007. Hypogene Speleogenesis: Hydrogeological and Morphogenetic Perspective. National Cave and Karst Research Institute, Carlsbad, NM.
- Klimchouk, A.B., 2009a. Morphogenesis of hypogenic caves. *Geomorphology* 106, 100–117. <https://doi.org/10.1016/j.geomorph.2008.09.013>.

- Klimchouk, A.B., 2009b. Epikarst: Hydrogeology, Morphogenesis, and Evolution. *Sonat, Simferopol*, 112 p. (in Russian).
- Klimchouk, A.B., 2015. The karst paradigm: changes, trends and perspectives. *Acta Carsologica* 44 (3), 289–313.
- Klimchouk, A.B., 2017. Types and settings of hypogene karst. In: Klimchouk, A., De Waele, J., Palmer, A.N., Auler, A.S., Audra, P. (Eds.), *Hypogene Karst Regions and Caves of the World*. Springer International Publishing AG, Cham, pp. 1–39.
- Klimchouk, A.B., 2019. Speleogenesis – hypogenic. In: White, W., Culver, D., Pipan, T. (Eds.), *Encyclopedia of Caves*, 3rd edition. Elsevier, pp. 974–988.
- Klimchouk, A.B., Ford, D.C., Palmer, A.N., Dreybrodt, W., 2000. Speleogenesis, Evolution of Karst Aquifers. National Speleological Society, Huntsville, Alabama, 527 p.
- Lipten, E.J., Smith, S.W., 2005. The geology of the Antamina Copper-Zinc deposit, Peru, South America. In: Porter, T.M. (Ed.), *Super Porphyry Copper & Gold Deposits: A Global Perspective*, v. 1. PGC Publishing, Adelaide, pp. 189–204.
- Love, D.A., Clark, A.H., Glover, J.K., 2004. The lithologic, stratigraphic, and structural setting of the giant Antamina copper–zinc skarn deposit, Ancash, Peru. *Econ. Geol.* 99, 887–916.
- Machare, J., Veliz, Y., Ortlieb, L., Dumont, J.-F., 1990. A review of recent paleoclimatic studies in Peru. In: Rabassa, J., Salemme, M. (Eds.), *Quaternary of South America and Antarctic Peninsula* 8. A.A. Balkema, Rotterdam, pp. 157–178.
- Mark, B., Stansell, N., Zeballos, G., 2017. The last deglaciation of Peru and Bolivia. *Cuad. Investig. Geogr.* 43 <https://doi.org/10.18172/cig.3265>.
- McKee, E.H., Noble, D.C., Scherkenbach, D.A., Drexler, J.W., Mendoza, J., Eyzaguirre, V. R., 1979. Age of porphyry intrusion, potassic alteration, and related Cu-Zn skarn mineralization, Antamina district, northern Peru. *Econ. Geol.* 74, 928–930.
- McKenzie, 2012. Peru expedition rewrites list of the world's highest caves. <http://cavingnews.com/2012/11/12/peru-expedition-rewrites-list-of-the-worlds-highest-caves>. (Accessed 1 November 2019).
- McNulty, B.A., Farber, D.L., Wallace, G.S., Lopez, R., Palacios, O., 1998. Role of plate kinematics and plate-slip-vectors partitioning in continental magmatic arcs: evidence from the Cordillera Blanca, Peru. *Geology* 26, 827–830.
- Mrozek, S.A., 2018. The Giant Antamina Deposit, Peru: Intrusive Sequence, Skarn Formation, and Mineralisation. James Cook University.
- Mrozek, S.A., Chang, Z., Meinert, L.D., 2015. A model for the intrusive sequence and Cu-Zn skarn formation at the Antamina deposit, Peru. In: *Proceedings of PACRIM 2015 Congress*, 18–21 March 2015, Hong Kong, China, pp. 423–429.
- Mrozek, S.A., Chang, Z., Meinert, L.D., Creaser, R.A., 2017. The Antamina deposit, Peru: U-Pb and Re-Os age constraints on magmatic-hydrothermal activity. In: *Conference Abstract FUTORES II (Future Understanding of Tectonics, Ores, Resources, Environment and Sustainability)*, Townsville, Queensland, Australia, 4 - 7 June 2017.
- Mukasa, S.B., 1984. Comparative Pb Isotope Systematics and Zircon U-Pb Geochronology for the Coastal, San Nicolas and Cordillera Blanca Batholiths of Peru. University of California, Santa Barbara.
- Palmer, A.N., 2007. *Cave Geology*. Cave Books, Dayton, OH.
- Perry, S.E., Garver, J.I., 2004. Onset of tectonic exhumation of the Cordillera Blanca, Northern Peru, based on fission-track and U-Th/He dating of zircon. *Geol. Soc. Am. Abstr. Programs* 36, 92.
- Petford, N., Atherton, M.P., Halliday, A.N., 1996. Rapid magma production rates, underplating and remelting in the Andes: isotopic evidence from northern-Central Peru (9°–11° S). *J. S. Am. Earth Sci.* 9, 69–78.
- Pfiffner, O.A., Gonzalez, L., 2013. Mesozoic-Cenozoic evolution of the western margin of South America: case study of the Peruvian Andes. *Geosciences* 3, 262–310.
- Pumacocha 2004 Expedition Report. http://cuevasdelperu.org/publicaciones/peru/2004_Pumacocha2004.pdf. (Accessed 1 November 2019).
- Ramos, V.A., 2009. Anatomy and global context of the Andes: main geologic features and the Andean orogenic cycle. Backbone of the Americas: shallow subduction, Plateau Uplift, and Ridge and Terrane Collision. *Geol. Soc. Am. Mem.* 204, 31–65. [https://doi.org/10.1130/2009.1204\(02\)](https://doi.org/10.1130/2009.1204(02)).
- Redwood, S.D., 2004. Geology and development history of the Antamina copper-zinc skarn deposit, Peru. In: *Society of Economic Geologists, Special Publication*, 11, pp. 259–277.
- Scherrenberg, A.F., Holcombe, R.J., Rosenbaum, G., 2014. The persistence and role of basin structures on the 3D architecture of the Marañón Fold-Thrust Belt, Peru. *J. S. Am. Earth Sci.* 51, 45–58.
- Seltzer, G.O., 1990. Recent glacial history and paleoclimate of the Peruvian-Bolivian Andes. *Quat. Sci. Rev.* 9 (2/3), 137–152.
- Spötl, C., Dublyansky, Y., Koltai, G., Honiat, C., Plan, L., Angerer, T., 2021. Stable isotope imprint of hypogene speleogenesis: lessons from austrian caves. *Chem. Geol.* 572, 120209.
- SRK Technical Report, 2016. Structural Study and 3-D Model of the Antamina Mine, Peru.
- SWS Technical Report, 2013. Hydrogeological Study of the Tucush Karst.
- Villarreal, E., Rivera, R., Santisteban, A., 2010. Características metalogénicas de la Cordillera Occidental en la Región Ancash. XV Congreso Peruano de Geología, Cusco, 27 setiembre - 1 octubre 2010. Resúmenes extendidos. *Publicación Especial* 9.
- Wise, J.M., Noble, D.C., 2003. Geomorphic evolution of the Cordillera Blanca, northern Peru. *Bol. Soc. Geol. Perú* 96, 65–85.
- Worthington, S., Ford, D., 2009. Self-organized permeability in carbonate aquifers. *Ground Water* 47 (3), 326–336. <https://ngwa.onlinelibrary.wiley.com/doi/full/10.1111/j.1745-6584.2009.00551.x>.
- Worthington, S.R.H., Ford, D.C., Beddows, P., 2000. Porosity and permeability enhancement in unconfined carbonate aquifers as a result of solution. In: Klimchouk, A., Ford, D., Palmer, A., Dreybrodt, W. (Eds.), *Speleogenesis: Evolution of Karst Aquifers*. Natl. Speleol. Soc, Huntsville, pp. 423–432.
- Zech, R., Smith, J.A., Kaplan, M., 2009. Chronologies of the Last Glacial Maximum and its Termination in the Andes (~10–55S) based on surface exposure dating. In: Vimeux, F., Sylvestre, F., Khodri, M. (Eds.), *Past Climate Variability in South America and Surrounding Regions, Developments in Paleoenvironmental Research*, 14. Springer, pp. 61–87. https://doi.org/10.1007/978-90-481-2672-9_3.